Advances in Water Resources 180 (2023) 104537

Contents lists available at ScienceDirect

Advances in Water Resources

journal homepage: www.elsevier.com/locate/advwatres

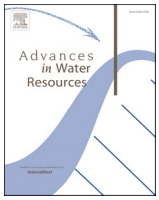

An adaptive multi-fidelity optimization framework based on co-Kriging surrogate models and stochastic sampling with application to coastal aquifer management

Vasileios Christelis [a,*], George Kopsiaftis [b], Rommel G. Regis [c], Aristotelis Mantoglou [b]

[a] British Geological Survey, Nicker Hill, Keyworth, Nottingham NG12 5GG, UK
[b] Laboratory of Reclamation Works and Water Resources Management, School of Rural, Surveying and Geoinformatics Engineering, National Technical University of Athens, 9 Iroon Polytechniou St., Zografou 15780, Athens, Greece
[c] Saint Joseph's University, Philadelphia, PA, 19131, USA

ARTICLE INFO

Keywords:
Pumping optimization
Surrogate modelling
Multi-fidelity
Coastal aquifers
Co-Kriging

ABSTRACT

Surrogate modelling has been used successfully to alleviate the computational burden that results from high-fidelity numerical models of seawater intrusion in simulation-optimization routines. Nevertheless, little attention has been given to multi-fidelity modelling methods to address cases where only limited runs with computationally expensive seawater intrusion models are considered affordable imposing a limiting factor for single-fidelity surrogate-based optimization as well. In this work, a new adaptive multi-fidelity optimization framework is proposed based on co-Kriging surrogate models considering two model fidelities of seawater intrusion. The methodology is tailored to the needs of solving pumping optimization problems with computationally expensive constraint functions and utilizes only small high-fidelity training datasets. Results from both hypothetical and real-world optimization problems demonstrate the efficiency and practicality of the proposed framework to provide a steep improvement of the objective function while it outperforms a comprehensive single-fidelity surrogate-based optimization method. The method can also be used to locate optimal solutions in the region of the global optimum when larger high-fidelity training datasets are available.

1. Introduction

There are several characteristics that define the fidelity of a physics-based numerical model and the interpretation is mainly problem dependent (Razavi et al. (2012),Asher et al., (2015) and references therein). Typically, a high-fidelity (HF) numerical model of a physical system considers the important processes and boundary conditions that represent reality as close as possible or includes those features that justify an acceptable accuracy for simulating the processes of interest (Giselle Fernández-Godino et al., 2019). Low or lower fidelity (LF) models can be defined for the same system by omitting part of the physics, by reducing the dimensionality of a 3D process to 2D, or even using the HF model but with relaxed convergence criteria or coarser spatial discretization (Razavi et al., 2012). As expected, the higher the complexity of the numerical model the longer it takes to simulate the system which in turn hinders the implementation of repetitive simulations tasks such as optimization.

In many water resources management studies, surrogate modelling has been an effective approach to confront the associated computational burden arising from HF and computationally expensive physics-based models (Castelletti et al., 2012; Wang et al., 2014; Song et al., 2018; Lim, 2021; Soleimani et al., 2021). However, when the HF numerical model is of substantial computational cost, only a few simulations might be considered affordable to provide the training dataset for constructing the surrogate models. In such cases, surrogate-based optimization (SBO) methods that only rely on HF data (single-fidelity) might struggle to return a satisfactory solution for the optimization problem at hand (Giselle Fernández-Godino et al., 2019). This complication that results from time-consuming HF numerical simulations can be tackled with the use of multi-fidelity or variable-fidelity optimization methods (Robinson et al., 2006). Moreover, the available computational budget for the HF model runs could indicate whether it is more efficient to choose a single-fidelity or a multi-fidelity SBO framework (Giselle Fernández--Godino et al., 2019).

* Corresponding author.
E-mail address: vc@bgs.ac.uk (V. Christelis).

https://doi.org/10.1016/j.advwatres.2023.104537
Received 12 January 2023; Received in revised form 13 July 2023; Accepted 5 September 2023
Available online 9 September 2023

Often, the exploration of the optimal search space may be informed by simpler, computationally efficient models which simulate the physical system at a LF level (Forrester et al., 2008). Within a multi-fidelity optimization framework, multiple simulations from faster LF models provide information on the general trends of the objective/constraint functions while fewer HF model runs improve the accuracy of the so-called multi-fidelity surrogate models. The latter, are constructed by considering the discrepancies among the various model fidelities to obtain a fast predictor that approximates the more accurate HF model (Zhou et al., 2020). Various studies have proposed different approaches to build multi-fidelity surrogates such as scaling functions based on Kriging or radial basis functions models (RBF) (Gano et al., 2004; Tyan et al., 2015; Song et al., 2019), co-RBF models (Durantin et al., 2017), polynomial chaos expansion (Man et al., 2021), hierarchical Kriging (Cheng et al., 2022), or co-Kriging models (e.g., Forrester et al., 2007; Le Gratiet and Garnier, 2014; Perdikaris et al., 2015; Perdikaris et al., 2017; Zhou et al., 2020).

In general, multi-fidelity optimization methods are essential when the HF data cannot be obtained in manageable CPU-time to construct single-fidelity surrogate models (Koziel and Leifsson, 2016). As with single-fidelity SBO, it is important that a sampling strategy, based on appropriate infill criteria, is utilized to adaptively locate the additional promising points, that will be evaluated with the physics-based models, other than the training points obtained from the initial sampling plan. Many papers in engineering optimization have explored such strategies in multi-fidelity optimization by developing variants of popular infill sampling criteria (e.g. Liu et al., 2016; Pellegrini et al., 2018; J. Zhang et al., 2018; Jiao et al., 2019; Serani et al., 2019; Shi et al., 2020; Yi et al., 2020; Cheng et al., 2022). Despite the successful application of multi-fidelity surrogates in other engineering disciplines, Razavi et al., (2012) and Asher et al., (2015) in their review papers noted that these methods have been less explored than the corresponding single-fidelity surrogates in water resources optimization studies. However, recently, multi-fidelity modelling has started seeing a growing interest in environmental applications with examples in CO_2 sequestration (Bianchi et al., 2016), inverse modelling (Y. Zhang et al., 2018; Xiao and Tian, 2020; Kreitmair et al., 2022), data assimilation (Zheng et al., 2019), hydrodynamic simulations (Moreno-Rodenas et al., 2018), brine transport simulation (Christelis and Hughes, 2022), pollution source identification on surface waters (Wu et al., 2020), flow and heat transport modelling (Menberg et al., 2020; Man et al., 2021) or flood reconstruction simulations (Bomers et al., 2019).

Pumping optimization of coastal aquifers is one of those widely addressed water resources management problems where the HF simulations of seawater intrusion, based on variable density flow and solute transport models (VDST), are computationally intensive. The numerical simulation is based on the solution of a non-linear coupled system of the partial differential equations for flow and solute transport in porous media that leads to long execution times (Younes et al., 2009; Hamzehloo et al., 2022). The coupling of VDST models with evolutionary algorithms is a rigorous approach to calculate optimal pumping rates for coastal aquifer management while literature suggests that evolutionary algorithms are highly competent to escape local optima and provide near global solutions, at the cost of thousands of objective function evaluations with the seawater intrusion model (Mantoglou et al., 2004; Ketabchi and Ataie-Ashtiani 2015b). Therefore, the overall computational cost can be prohibitive to employ a simulation-optimization routine, which depends also on the number of the decision variables (curse of dimensionality). It is fair to assume, that for a regional real-world coastal aquifer this task appears computationally intractable without resorting to code parallelization, which evidently requires additional resources and effort to set it up (Ketabchi and Ataie-Ashtiani, 2015a).

Similar to other water resources optimization studies, single-fidelity SBO methods have been successfully applied in coastal aquifer management problems by using various sampling frameworks and types of surrogate models (e.g., Sreekanth and Datta, 2010; Ataie-Ashtiani et al., 2014; Christelis et al., 2018; Lal and Datta, 2018; Roy and Datta, 2019; Yin and Tsai, 2020; Siade et al., 2020; Yu et al., 2021). However, a common assumption, adopted in previous studies of SBO for coastal aquifer management, is that a reasonable amount of HF training data can be obtained from VDST simulations. Several LF models of seawater intrusion have been developed to approximate coastal aquifer flow at a different accuracy level and computational efficiency (e.g., Strack, 1976; Bakker, 2003; Bakker et al., 2004; Koussis et al., 2012; Koussis et al., 2015; Rozos et al., 2021). Nevertheless, only a few studies have examined, so far, the fusion of HF data from VDST models and LF data from LF models of seawater intrusion for pumping optimization problems of coastal aquifers.

For example, Christelis and Mantoglou (2016) developed an optimization strategy embedded within the operations of an evolutionary algorithm where two model fidelities of seawater intrusion were considered, a sharp interface model and the VDST model. Their approach was based on an adaptive adjustment of the buoyancy ratio to smooth out the differences of the constraint functions between the two model fidelities. That was, to the best of our knowledge, the first study that combined seawater intrusion models of different fidelities for solving pumping optimization problems in coastal aquifers and has similarities to the implicit space mapping techniques (Bandler et al., 2004). The advantage of that method is that it locates feasible solutions within a few iterations of the optimization algorithm, but it can easily get trapped on local minima and for certain sets of aquifer parameters it will unnecessarily utilize runs from the VDST model (Christelis, 2021).

Christelis and Mantoglou (2019) applied simple response corrections for the constraints of the sharp interface model based on radial basis functions to match the response of the VDST model. That multi-fidelity optimization framework was compared to a single-fidelity SBO method but did not offer notable advantages for a HF computation budget that was equal to ten times the number of the decision variables of the optimization problem. Dey and Prakash (2020) developed a similar methodology to Christelis and Mantoglou (2016) for a real-world coastal aquifer in India. Their approach also showed significant computational gains and located feasible solutions for the VDST-based optimization that were also better than using the LF sharp interface model alone. Christelis (2021) proposed a multi-fidelity optimization method for coastal aquifer management based on co-Kriging surrogate models. That method provided promising results, but it was only based on a prediction-based exploitation strategy that can get trapped on local minima. Also, it was tested against single-fidelity SBO methods for very small HF training datasets, which is a favourable condition for multi-fidelity optimization.

Clearly, multi-fidelity optimization has received little attention for coastal aquifer management and there is a need to further explore those methods for cases where only a limited number of VDST model runs is affordable due to high computational cost. For example, this situation can be encountered in real-world VDST models developed over large spatial scales with complex boundary conditions and many pumping wells. Such features can have an adverse effect on the application of single-fidelity surrogate models for limited HF training data. In the present study, we build upon our previous work on adaptive single-fidelity SBO frameworks (Regis, 2011,2014a) as well as on single- and multi-fidelity SBO for coastal aquifer management (Christelis et al., 2018; Christelis, 2021). Our motivation stems from the practical need to develop an efficient and robust approach that locates feasible solutions for pumping optimization problems of coastal aquifers with computationally expensive constraint functions when only a small number of VDST model runs is considered affordable.

To achieve that, we propose a multi-fidelity optimization framework that utilizes individual co-Kriging surrogate models to emulate the response of the constraint functions and an adaptive stochastic sampling strategy to evaluate promising candidate points with the computationally expensive VDST model. The method of co-Kriging, which is a special formulation of Kriging, differs from a typical surrogate model in the

sense that it amalgamates data from at least two models (usually a larger amount of LF data and much fewer HF data), in order to develop a multi-fidelity surrogate of the HF numerical model (Forrester et al., 2007). Given an adequate training sample and a good correlation between the LF and the HF model response, the co-kriging surrogate model is expected to predict the HF model response more accurately than using the LF model alone. It is also noted that many studies, in other engineering disciplines, employ constrained SBO through the use of the probability of feasibility function, but much fewer studies apply direct handling of constraints either using single- or multi- fidelity surrogate models (e.g., Regis, 2011,2014; Cheng et al., 2022). Furthermore, there is little existing literature on coastal aquifer management and SBO strategies that consider balanced exploration and exploitation adaptive schemes (Song et al., 2018; Christelis 2021). Ideally, a SBO strategy should update the accuracy of the surrogate models, after the initial training, either by focusing on new points in the region of the optimum that the surrogate models predict (local exploitation) or by improving their general accuracy with training data away from current known optimal points (global exploration) (Forrester et al., 2008). While this is challenging to achieve, particularly when the HF data are limited, developing a balanced exploitation/exploration scheme that is controlled by appropriate criteria enables the global search capabilities of the SBO algorithm.

The proposed multi-fidelity SBO scheme of this work employs a merit function that can balance local exploitation and global exploration while it also adopts an online correction of the LF model to handle acknowledged discrepancies between sharp interface and VDST models. We explore different approaches for generating infill points after the initial training design and how optimization performance is related to increasing HF and LF computational budgets. For performance comparison, the proposed multi-fidelity SBO approach is compared to a comprehensive single-fidelity SBO algorithm that has previously demonstrated a robust performance on pumping optimization of coastal aquifers within small HF training points (Christelis et al., 2018). This enables a better understanding of the practicality of multi-fidelity methods in pumping optimization of coastal aquifers in comparison to the less complicated and faster approach of single-fidelity SBO algorithms. All SBO methods that are employed in this work are applied first for a hypothetical 3D coastal aquifer model to facilitate the run of multiple independent optimization trials and obtain sample statistics. Then, we evaluate the proposed method on a pumping optimization problem for a real-world 3D coastal aquifer model of the Vathy coastal aquifer located in the Greek island Kalymnos in the Aegean Sea.

2. Seawater intrusion models and optimization problem

As discussed in the introduction part, various mathematical models are available to simulate seawater intrusion at different levels of accuracy and sophistication. For the purposes of the present study, we employ two model fidelities, that is, a 3D VDST numerical model that represents the HF option for simulating seawater intrusion and a 2D sharp interface model that is the LF option. The latter neglects mixing of freshwater with seawater and only considers a 2D one-fluid aquifer flow. Therefore, the LF model utilized here omits part of the coastal aquifer flow physics and it is also of reduced dimensionality. Depending on the problem at hand, different HF and LF models can be considered for implementation with the proposed multi-fidelity framework. In the sections that follow, we describe the two model fidelities selected for simulating seawater intrusion, the application models, and the formulation of the pumping optimization problem.

2.1. The HF model

In this study, the finite-difference numerical code SEAWAT-version 4 (Langevin and Guo, 2006) was used to simulate seawater intrusion based on the VDST model. A brief description of the governing equations of the VDST model is presented, assuming that density is affected only by concentration while thermal and viscosity effects are neglected. The following flow and solute transport differential equations are coupled, as the density across the dispersive zone varies from that of freshwater ($\approx 1000 \mathrm{kg}/\mathrm{m}^3$) to that of seawater ($\approx 1025\,\mathrm{kg}/\mathrm{m}^3$).

$$-\nabla\cdot(\rho\mathbf{q}) + \rho_s q_s = \rho S_f \frac{\partial h_f}{\partial t} + n\frac{\partial \rho}{\partial C}\frac{\partial C}{\partial t} \tag{1}$$

$$\frac{\partial C}{\partial t} = \nabla\cdot(\mathbf{D}\cdot\nabla C) - \nabla\cdot(\mathbf{v}C) - \frac{q_s}{n}C_s \tag{2}$$

where the variables ρ and ρ_s represent the fluid density and the density of water entering or leaving the system through a source or sink. The specific discharge vector $\mathbf{q}$ and the volumetric flow rate per unit volume of porous medium representing sources and sinks q_s, are the other two terms of the left part of Eq. (1). On the right hand side, h_f is the equivalent freshwater head, t represents time, specific storage is S_f, n is the porosity while solute concentration is denoted by C. The first term, in the right hand side of Eq. (2) is the hydrodynamic dispersion term with $\mathbf{D}$ being the hydrodynamic dispersion tensor, and the second term describes advection, with $\mathbf{v}$ being the fluid velocity vector, while C_s is the solute concentration of water entering or leaving through sources and sinks, respectively.

The specific discharge term, for variable-density flow with constant viscosity, is calculated using Darcy's law with the components of specific discharge expressed along the principal directions of anisotropy for hydraulic conductivity K_x, K_y and K_z, as:

$$\begin{aligned} q_x &= -K_{fx}\left(\frac{\partial h_f}{\partial x}\right) \\ q_y &= -K_{fy}\left(\frac{\partial h_f}{\partial y}\right) \\ q_z &= -K_{fz}\left(\frac{\partial h_f}{\partial z} + \frac{\rho-\rho_f}{\rho}\right) \end{aligned} \tag{3}$$

with the freshwater density denoted as ρ_f and q_x, q_y, q_z and K_{fx}, K_{fy}, K_{fz} representing the components of the specific discharge and the components of freshwater hydraulic conductivity along the principal directions, respectively. Fluid density depends on solute concentration through the following relationship:

$$\rho = \rho_o\left(1 + \frac{\varepsilon}{(C_s - C_o)}(C - C_o)\right) \tag{4}$$

where ρ_o is the reference density, C_o is the reference concentration and C_s is the maximum concentration, which for this work take the values $C_o = 0 kg/m^3$ for freshwater and $C_s = 35\,kg/m^3$ for seawater. The buoyancy ratio is expressed as $\varepsilon = (\rho_s - \rho_o)/\rho_o$ with $\rho_o = \rho_f$ for the case of freshwater while ρ_s corresponds to maximum seawater density.

2.2. The LF model

The lower fidelity model employed here adopts the Dupuit approximation and it is based on the sharp interface assumption where only flow in the freshwater zone is considered (one-fluid approach). The model neglects spatial density variability, aquifer flow is horizontal and steady-state, there is no mixing between freshwater and saltwater and the discharge potential formulation is applied (Strack 1976). The depth to the interface is estimated using the Ghyben-Herzberg approximation. For irregularly shaped aquifers with spatially variable hydraulic conductivity and recharge, this analytical model can be solved using a numerical groundwater flow code with minimal computational requirements as only a steady-state flow equation is solved for either confined or unconfined aquifers (Mantoglou et al., 2004).

$$\begin{aligned} &\frac{\partial}{\partial x}\left(K\frac{\partial \Phi}{\partial x}\right)+\frac{\partial}{\partial y}\left(K\frac{\partial \Phi}{\partial y}\right)-Q(x,y)=0, && \text{confined interface flow}\\ &\frac{\partial}{\partial x}\left(K\frac{\partial \Phi}{\partial x}\right)+\frac{\partial}{\partial y}\left(K\frac{\partial \Phi}{\partial y}\right)+N-Q(x,y)=0, && \text{unconfined interface flow} \end{aligned} \tag{5}$$

where K is the aquifer's horizontal hydraulic conductivity,Nrepresents the rate of groundwater recharge for the case of unconfined aquifer flow and the term $Q(x, y)$ denotes the distributed pumping rate. The discharge potential Φ is calculated separately for confined and unconfined flow (Strack, 1976; Mantoglou et al., 2004) while its value Φ_{toe} at the location of the interface toe is of particular interest in pumping optimization problems and is calculated as (Mantoglou, 2003):

$$\left.\begin{aligned} \Phi_{toe}&=\frac{\varepsilon}{2}B^2, && \text{confined aquifer}\\ \Phi_{toe}&=\left[\frac{\varepsilon(\varepsilon+1)}{2}\right]d^2, && \text{unconfined aquifer} \end{aligned}\right\} \tag{6}$$

where B is aquifer thickness and variable d is the vertical distance from sea level to the aquifer base. The discharge potential is generally defined as $\Phi=\frac{1}{2}\mathrm{K}\frac{\rho_s}{(\rho_s-\rho_f)}(\phi-H_{sea})^2+C_{const}$, where ϕ denotes the freshwater hydraulic head, $H_{sea}=B$ for confined flow and $H_{sea}=d$ for unconfined flow, while C_{const} is a constant that ensures that Φ is single-valued throughout the aquifer (Koussis et al., 2012).

2.3. Hypothetical application

The hypothetical coastal aquifer model (Fig. 1) refers to an unconfined coastal aquifer of a simple orthogonal shape geometry with horizontal dimensions $X=7000m$, $Y=3000m$ and an horizontal aquifer base set at $z=25m$ below sea level.

A finite difference grid is applied with $dx=dy=50m$ for each of the five layers of the 3D VDST numerical model. Hydrostatic boundary conditions are applied at the left side of the aquifer model to represent the hydraulic connection with the sea, based on a saltwater density of $1025Kg/m^3$and a specified constant salinity concentration of $35\,Kg/m^3$. A homogeneous and anisotropic hydraulic conductivity is assumed with $K_{fx}=K_{fy}=50m/day$ and $K_{fz}=5m/day$, while the longitudinal, transverse, and vertical transverse dispersivity values are set correspondingly to $\alpha_L=25m$, $\alpha_T=2.5m$ and $\alpha_{TV}=0.25m$. A daily average surface recharge of $3x10^{-4}m/day$ replenishes the aquifer at the top model layer while ten fully penetrating pumping wells extract groundwater based on daily average rates for a management simulation period of 30 years. This 3D hypothetical model with a runtime of approximately 25 s enabled multiple VDST simulations at a manageable computational cost given

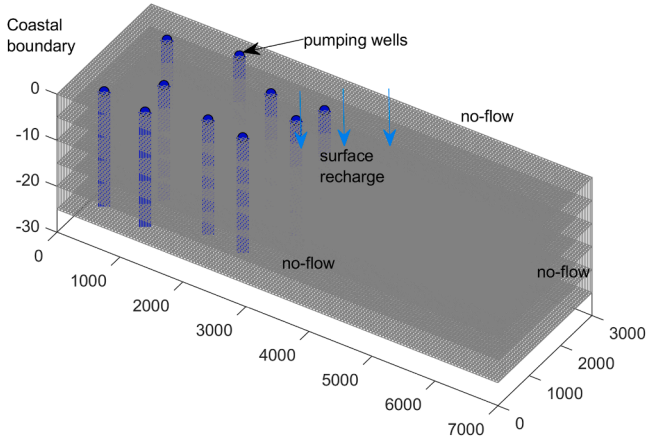

Fig. 1. Hypothetical coastal aquifer model with applied boundary conditions and location of pumping wells (in blue color).

that a total of 30 independent optimization trials were considered for each framework to obtain meaningful sample statistics on their performance. The corresponding LF sharp interface model, which is a 2D model, takes only 0.31 s to solve for the discharge potential Eq. (5) offering a significant decrease in computational time.

2.4. Real-world application

Our real-world application is an unconfined aquifer located at the central part of Kalymnos Island, Greece, situated in the eastern Mediterranean region (Fig. 2).

The elongated shaped aquifer follows the WNW – ESE orientation of the Vathy valley and mainly consists of carbonate rocks (e.g., limestones and marbles), that cover perimetrically more than 70% of the surface area. The central area of the aquifer could be divided in three lithological units, which in descending order of permeability- are the following: 1) scree, 2) alluvial deposits and 3) tuff (Mantoglou et al., 2004). According to the available borehole logging data, the aquifer is bounded at the bottom by an impermeable schist unit at the depth of 25 m below sea level. The sea boundary is in the east side of the aquifer, while the remaining boundaries are considered impermeable. The recharge rates vary from 30 mm/year to 150 mm/year according to the hydro-lithological characteristics of the rock formations. The recharge zones coincide with the lithological units described above. Overall, the coastal aquifer model includes 4 separate zones of hydraulic conductivity and recharge. A single runtime with the Kalymnos 3D VDST model is approximately 2.5 min while the corresponding 2D sharp interface model simulates aquifer flow in 1.6 s.

2.5. Formulation of the pumping optimization problem

The control of seawater encroachment while satisfying the demand for freshwater in coastal regions is a common groundwater management problem with approaches varying from standard simulation-optimization methodologies (Sreekanth and Datta, 2015) to game theory (Nagkoulis and Katsifarakis, 2022). Here, we solve a simulation-optimization problem where the decision variables are the individual pumping rates Q_i, $i=1, \ldots, k$ with k being the total number of pumping wells. We wish to maximize the objective function $f(\mathbf{Q})$, where $\mathbf{Q}=(Q_1,\ldots, Q_k)$ is a decision vector of pumping rates, subject to a set of constraints g_j, $j=1, \ldots, 2k$ that monitor the extent of seawater intrusion and the groundwater levels and satisfy certain criteria for each pumping well. For our study, the mathematical formulation of the VDST-based optimization is:

$$\begin{aligned} &\min -\sum_{i=1}^{k} Q_i\\ &s.t.\ \ x_i^{C_t}(Q_1,\ldots,Q_k)\le xw_i, \forall i=1,\ldots,k\\ &\quad h_i(Q_1,\ldots,Q_k)\ge 0, \forall i=1,\ldots,k\\ &\quad Q_{\min}\le Q_i\le Q_{\max}, i=1,\ldots,k \end{aligned} \tag{7}$$

where $x_i^{C_t}(Q_1,\ldots,Q_k)$ represents the extent of seawater intrusion based on the isosalinity contour with a value equal to the threshold C^t as a function of the pumping rates. It is marginally allowed for $x_i^{C_t}$ to reach the *ith* pumping well location xw_i. Similarly, the piezometric head h_i at the *ith* pumping well should remain at a level greater than or equal to zero with respect to sea level. The variables $Q_{\min}$ and $Q_{\max}$ are the lower and upper values that can be assigned to pumping rates during optimization. It is noted that the negative sign in front of the objective function in Eq. (7) indicates maximization given that the location of the maximum $f(\mathbf{Q}^*)$ lies at the same point with the minimum $-f(\mathbf{Q}^*)$. The objective function is linear with respect to the decision variables and computationally cheap to evaluate but the inequality constraints h_i and $x_i^{C_t}$ are non-linear with respect to pumping rates because of the

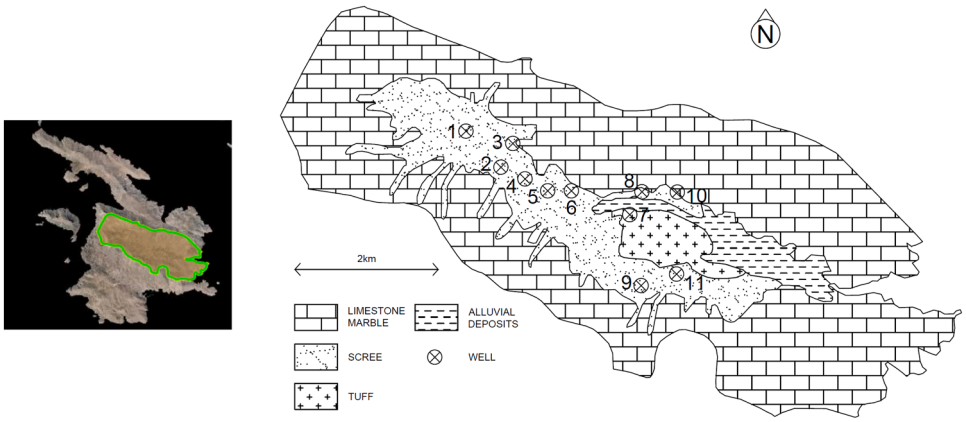

Fig. 2. The Vathy aquifer in Kalymnos Island along with the location of the pumping wells and the distribution of the geological materials.

equations that govern the VDST model formulation and are obtained from computationally expensive simulations with that model.

While the VDST simulations provide a salinity concentration field, the output from the sharp interface model is the potential flow field where the interface location is indirectly calculated using linear interpolation and the value of Φ_{toe} from Eq. (6). Hence, the corresponding optimization problem for the sharp interface model is formulated as:

$$\begin{aligned} &\min -\sum_{i=1}^{k} Q_i \\ &s.t.\ x_i^{\Phi_{toe}}(Q_1,\ldots,Q_k) \le xw_i, \forall i = 1,\ldots,k \\ &\quad \Phi_i(Q_1,\ldots,Q_k) \ge 0, \forall i = 1,\ldots,k \\ &\quad Q_{\min} \le Q_i \le Q_{\max}, i = 1,\ldots,k \end{aligned} \tag{8}$$

where $x_i^{\Phi_{toe}}(Q_1,\ldots,Q_k)$denotes the extent of seawater intrusion based on the location of the interface toe as a function of the pumping rates. In analogy with the VDST model it is also marginally allowed for $x_i^{\Phi_{toe}}$ to reach the *ith* pumping well location xw_i while Φ_i, which is the discharge potential at the *ith* pumping well, should also remain at a level greater than or equal to zero with respect to sea level.

The above pumping optimization problems can be solved using a direct approach by combining the HF VDST or the LF sharp interface model with an evolutionary algorithm. Here, we employ the evolutionary annealing-simplex (EAS) algorithm (Efstratiadis and Koutsoyiannis 2002) which has demonstrated global exploration capabilities in both smooth and rugged search spaces (Tsoukalas et al., 2016) and an efficient and robust performance in pumping optimization of coastal aquifers (Christelis et al., 2019; Kopsiaftis et al., 2019). To enable the direct optimization using the EAS algorithm the nonlinear constraints were embedded into the objective function by using penalty terms. This is expressed below for the HF case similar to Christelis et al., (2018):

$$f(\mathbf{Q}) = \begin{cases} -\sum_{i=1}^{k} Q_i, \ if\ \forall j;\ \left(g_H^j(\mathbf{Q}) \le 0\right), j = 1,\ldots,2k \\ M_g \sum_{j=1}^{2k} \left[\max\left(g_H^j, 0\right)\right]^2, \ if\ \exists j;\ \left(g_H^j(\mathbf{Q}) > 0\right), j = 1,\ldots,2k \end{cases} \tag{9}$$

where M_g represents the number of constraint function violations either for salinity or hydraulic head criteria or both. It is assumed that for a decision vector $\mathbf{Q}$, the HF constraint functions are summarized in $g_H^j(\mathbf{Q})$ and the corresponding LF constraint funtions in $g_L^j(\mathbf{Q})$ if we use the LF model alone to solve the pumping optimization problem.

3. Surrogate-based optimization

3.1. The surrogate models

The multi-fidelity optimization framework is based on the construction of individual co-Kriging (coKRG) surrogate models to approximate the response of the HF constraint functions using training data from both model fidelities for simulating seawater intrusion. The method of coKRG is an extension of Kriging that incorporates data from various model fidelities and it is an established surrogate modelling technique for multi-fidelity optimization applied in engineering problems and fluid mechanics (e.g., Forrester et al., 2007; Koziel et al., 2013, Singh et al., 2017; Ruan et al., 2020). We compare the multi-fidelity SBO against the ConstrLMSRBF algorithm (Regis, 2011). The latter is a single-fidelity SBO method, that has shown a strong performance for pumping optimization problems of coastal aquifers under limited computational budgets (Christelis et al., 2018). The version of the ConstrLMSRBF algorithm applied here requires that at least one feasible point exists among the initial training points and uses radial basis functions (RBF) as surrogate models of the constraints and the objective function.

Both coKRG and RBF models have interpolating capabilities that allow for an exact estimation of the previously evaluated sampling points with the original physics-based model. This feature has been successfully exploited in the development of adaptive SBO schemes for deterministic computer simulations of water resources systems (e.g., Müller and Woodbury, 2017; Xia and Shoemaker, 2020; Xia et al., 2021; Pang et al., 2022; Lu et al., 2022). In the next two sections we only briefly present the surrogate model predictors as more elaborative details on their mathematical formulation can be found elsewhere (e.g., Regis and Shoemaker, 2005; Forrester et al., 2007; Forrester and Keane, 2009). More emphasis is given to the practical application of those techniques for developing the SBO frameworks and the implications for coastal aquifer management.

First, we define the required variables for describing the surrogate model predictors based on the samples provided by both the HF and the LF physics-based models. Consider a set of n_H training points denoted as$X_H = [x_H^{(1)},\ldots,x_H^{(n_H)}] \in \mathbb{R}^k$ where we sample the HF numerical model (here, the VDST model). The corresponding model responses for all HF constraint functions (except bounds on decision variables) are summarized in the form $G_H^{(j)} = [g_H^j(\mathbf{x}_H^{(1)}),\ldots,g_H^j(\mathbf{x}_H^{(n_H)})]$ where $j = 1,\ldots,2k$ denotes the number of constraint functions which, for our study, is twice the number of pumping wells k. Similarly, consider a set of n_L training points denoted as $X_L = [x_L^{(1)},\ldots,x_L^{(n_L)}] \in \mathbb{R}^k$ that are used to run the sharp interface model and obtain the corresponding LF constraint functions summarized in the form $G_L^{(j)} = [g_L^j(\mathbf{x}_L^{(1)}),\ldots,g_L^j(\mathbf{x}_L^{(n_L)})]$. The HF and LF constraint functions are calculated in the form of $g(\mathbf{x}) \le 0$. For the

specific case of the multi-fidelity approach, X_H is typically a subset of the X_L training points (i.e., $X_H \subset X_L$).

Therefore, for the implementation of the ConstrLMSRBF algorithm and for each of the constraint functions the following RBF approximation is defined (Regis, 2011):

$$s(\boldsymbol{x}_H) = \sum_{j=1}^{n_H} \lambda_j \varphi\left(\| \boldsymbol{x}_H - \boldsymbol{x}_H^{(j)} \| \right) + p(\boldsymbol{x}_H), \boldsymbol{x}_H \in \mathbb{R}^k \tag{10}$$

where $\boldsymbol{\lambda} = [\lambda_1, ..., \lambda_{n_H}]^T \in \mathbb{R}^{n_H}$ are coefficients to be determined, $\| \cdot \|$ is the Euclidean norm and $\varphi(\cdot)$ is the basis function, which in our case takes the cubic form $\varphi(r) = r^3$ due to previous successful performance of this RBF type on pumping optimization problems of coastal aquifers (Christelis et al., 2018). The term $p(x_H)$ represents a linear polynomial tail whose coefficients along with the coefficients $\boldsymbol{\lambda}$ also need to be determined such that the resulting RBF model passes through all the n_H design points. The required coefficients are obtained by solving a linear system of equations while it is noted that at least $k + 1$ affinely independent points are required to train the RBF model (Regis and Shoemaker, 2013):

$$\begin{bmatrix} \boldsymbol{\Phi} & \mathbf{P} \\ \mathbf{P}^T & \mathbf{0}_{(k+1)\times(k+1)} \end{bmatrix} \begin{bmatrix} \lambda \\ \mathbf{w} \end{bmatrix} = \begin{bmatrix} G_H^i \\ \mathbf{0}_{(k+1)\times 1} \end{bmatrix} \tag{11}$$

where $\mathbf{P} \in \mathbb{R}^{n_H \times (k+1)}$ is a matrix so that the *ith* row is $[1, (x_H^i)^T]$, while $\boldsymbol{\Phi} \in \mathbb{R}^{n_H \times n_H}$ is a matrix with entries $\boldsymbol{\Phi}_{j,\,l} = \varphi(\|x_H^{(j)} - x_H^{(l)}\|)$, $j, l = 1, ..., n_H$ and $\mathbf{w} = (w_1, ..., w_{k+1})^T$ represents the coefficients of the linear polynomial $p(\mathbf{x}_H)$. The term $\mathbf{0}_{(k+1)\times(k+1)}$ is a zero matrix and $\mathbf{0}_{(k+1)\times 1}$ is a zero vector. The significant advantage of using RBF models with adaptive SBO methods is that their training time is computationally inexpensive even for large training datasets (Regis, 2011).

Following Forrester et al., (2007), we now consider also a combined set of low and HF points denoted as $X_{HL} = \begin{pmatrix} X_L \\ X_H \end{pmatrix}$ and the set of observed responses is defined as $G_{HL}^{(i)} = \begin{pmatrix} G_L^{(i)} \\ G_H^{(i)} \end{pmatrix}$. Similar to Kriging models, the value at a sampling point in X_{HL} is treated as generated by stochastic processes. The Gaussian process $Z_H(\cdot)$ and $Z_L(\cdot)$ are also defined to represent the local features of the HF and the lower fidelity models respectively, while the Gaussian process $Z_d(\cdot)$ represents the difference between $\beta Z_L(\cdot)$ and $Z_H(\cdot)$, where β is a scaling factor that multiplies the lower fidelity model and is estimated through optimization (Forrester et al., 2007). The approximation of the HF model in the coKGR formulation is expressed as (Forrester et al., 2008):

$$\hat{y}_H(x) = \hat{\mu} + c^T C^{-1}(y - 1\hat{\mu}) \tag{12}$$

where C represents a complex covariance matrix of the co-Kriging method, which now includes correlations between the HF X_H and LF data X_L and a set of hyper-parameters θ and p to be determined. The term c is defined as a vector of the covariance of X_{HL} and the point to be predicted x, $\hat{\mu}$ represents the maximum likelihood estimation of the mean and 1 denotes a vector of ones. A thorough analysis on the derivation of coKRG models for surrogate-based optimization can be found in Forrester et al., (2007) and Forrester et al., (2008) while the ooDACE MATLAB toolbox was used here for the development of the coKRG models (Couckuyt et al., 2014; Ulaganathan et al., 2015).

3.2. The multi-fidelity SBO framework

Our aim is to develop an optimization framework that considers both seawater intrusion model fidelities and returns optimal solutions that cannot be obtained by using the few HF runs or the LF model alone. As discussed in the introduction, it is challenging to obtain a steep improvement of the objective function while utilizing only a few HF model simulations due to the potential excess computational cost. For example, a global search based on a HF model, with runtimes in the order of hours, is computationally impractical on a desktop-based analysis. This is particularly difficult if other features co-exist such as increased dimensionality or a multi-modal objective function landscape. In fact, even attaining a good local feasible solution might be non-trivial under a limited HF computational budget. Therefore, a more focused framework is required to exploit as much information as possible from both model fidelities towards locating improved feasible solutions. An established method in Kriging-based frameworks is to define an auxiliary optimization problem that minimizes an acquisition function that involves infill criteria for identifying one or more promising points to evaluate with the HF model in an iterative fashion. These frameworks have demonstrated their global capabilities in many engineering optimization problems, but for our problem at hand and based on our preliminary computational experiments with these frameworks, a considerable number of iterations is required to return notable improvements of the objective function and thus, they do not address the scope of this study.

In a previous study, Christelis et al., (2018) showed that the single-fidelity ConstrLMSRBF algorithm (Regis, 2011) had a strong performance for a series of problems with increasing numbers of decision variables within small HF computational budgets (maximum was ten times the number of decision variables). ConstrLMSRBF follows a rather different concept compared to the approach of minimizing an acquisition function. In each iteration, a large random set of candidate solutions is generated by using normal distributions with zero mean on the current best HF solution and a standard deviation σ that varies depending on the progress of the algorithm. Therefore, perturbations of different magnitude around the current best solution are utilized to generate a set of candidate points and radial basis functions are used as surrogate models to provide a fast evaluation of those candidate solutions. The identification of the next promising point for evaluation with the HF model is based on a weighted score function that balances exploration with exploitation.

Here, the need is to locate feasible solutions using a quite small number of HF model runs, which favours the stochastic sampling strategy of ConstrLMSRBF for our multi-fidelity implementation. However, the application of multi-fidelity SBO methods is not always straightforward as the discrepancies between the LF and the HF model might negatively affect the successful implementation (Zhou et al., 2016). It is not uncommon that a much faster LF model can be quite inaccurate compared to the HF model. Indeed, in our case, it has been observed that the computationally cheap sharp interface model of Strack (1976) underestimates maximum allowed total pumping, as the extent of seawater intrusion is overestimated compared to the corresponding VDST simulation (Dausman et al., 2010; Pool and Carrera, 2011). A simple correction to that discrepancy was proposed by Pool and Carrera (2011) by reducing the buoyancy ratio ε through an empirical equation. This one-off correction of ε improves the generic match with the simulated dispersion zone from the VDST model but it should be controlled during optimization to ensure that the constraints of the HF VDST model are not violated (Christelis and Mantoglou, 2016; Kopsiaftis et al., 2019). Thus, it is not straightforward to identify which value of ε might be optimal to better align the response of the constraint functions of the sharp interface model to that of the VDST model for solving a pumping optimization problem when thousands of pumping rate combinations should be evaluated.

To that end, the multi-fidelity framework developed here combines the stochastic sampling strategy proposed in Regis (2011), the use of coKRG surrogate models for the constraint functions and the concept of adaptive correction of the buoyancy ratio, during the operations of a pumping optimization framework of coastal aquifers (Christelis and Mantoglou, 2016). As our proposed multi-fidelity SBO algorithm falls within the general category of adaptive-recursive frameworks, it will be henceforth named as Adaptive Recursive Optimization with Multi-fidelity Surrogates (AROMS). In AROMS, the LF model is first

evaluated on a large set of points provided by a space-filling design. How large this LF sample should be is problem-dependent but generally, the empirical rule of ten times the number of decision variables (Jones et al., 1998) is considered an adequate choice. A critical step is to select a subset of those LF points for evaluation with the HF model to obtain a necessary initial training sample (at least two HF points) to fit the parameters of the co-Kriging surrogate models. It is suggested to start with as low as two expensive HF points and let the next infill points to be found via the iterative framework of AROMS. Based on our several tests with AROMS framework, this minimal setting for the initial HF training points ensures a better performance than evaluating a larger subset and provides a more effective use of the limited HF model simulations. In our implementation, the values of the LF objective function are first sorted and the points that correspond to the best and second-best value are selected. If, based on the HF evaluation, none of those initial points are feasible, additional known feasible HF points should be provided even if the latter are a conservative solution far from the expected near global optima. It is possible to locate feasible solutions during the iteration steps of AROMS when none of the initial HF points are feasible, but this choice will worsen its performance.

Let N_L and N_{HF}^0 represent the number of the initially available LF and HF training points obtained before starting the iterations of the AROMS framework. Also, N_{HF} denotes the number of additional high-fidelity training points obtained at the N_{eval} iteration of AROMS and $N_{\max}$ is the maximum number of high-fidelity model runs (or interchangeably number of high-fidelity training points) that we can afford during optimization and it also defines the stopping criterion for the algorithm. The initial best feasible HF solution x_{best} is first identified from the set N_{HF}^0. Within the main loop of the AROMS algorithm, an essential part is to generate a large number $n_{cand} = \min\{1000k, 10000\}$ of promising candidate solutions $X_{cand} = [x_{cand}^{(1)}, \ldots, x_{cand}^{(n_{cand})}]$. These are generated by perturbing the current known best solution x_{best}, as indicated from the previous evaluations with the HF model, using normal distributions with zero mean and standard deviation σ. The latter varies between a minimum and a maximum value and depends on the progress of the algorithm in terms of the number of successful iterations in locating a new x_{best}, as described in the ConstrLMSRBF framework (Regis, 2011).

Every time an updated x_{best} is identified, a secondary optimization problem is occasionally solved, within AROMS operations, that seeks for an optimal buoyancy ratio ε* that minimizes the following metric:

$$g_{diff}(\varepsilon^*) = \sqrt{\left[\sum \left(g_H^j(x_{best}) - g_L^j(x_{best}, \varepsilon^*)\right)^2 \Big/ k\right]} \tag{13}$$

That is, a root mean square error metric g_{diff} that considers the difference between the constraint functions calculated from the LF sharp interface model g_L^j and those of the HF model g_H^j with $j = 1, \ldots, 2k$ at the current optimum solution x_{best}. A new updated value for ε* is obtained based on the MATLAB's *fminbnd* function (Optimization Toolbox 2021) that finds the minimum of a single-variable function (Eq. (13)) on a fixed interval $\varepsilon_{lb} < \varepsilon^* < \varepsilon_{ub}$ where $\varepsilon_{lb} = 0.0079$ and $\varepsilon_{ub} = 0.025$ in our case. The value of ε_{lb} is based on the Pool and Carrera (2011) empirical equation while ε_{ub} is the standard buoyancy ratio for freshwater and saltwater. After finding an optimal value for the buoyancy ratio at x_{best}, the LF model re-evaluates the available LF points, which facilitates the construction of more accurate coKRG models, as the constraints of the LF model are now better correlated with that of the HF model. Obviously, if it is known a priori that the response of the chosen LF model correlates well with that of the HF model, then the coKRG surrogate models can be constructed for the constraint functions without the need for extra LF corrections and the main iterative framework of AROMS is directly applied.

The computationally expensive constraint functions are calculated using the coKRG surrogate models on all the candidate points X_{cand} whereas the computationally cheap objective function is calculated as in Eq. (9) to provide the vector of $\widehat{\mathbf{y}}(X_{cand})$ values. The next promising point to evaluate with the HF model is selected based on the weighted score of a merit function that seeks to balance exploration with exploitation and has the following form:

$$F_a(X_{cand}) = w_{cr}\widehat{y}_{sc}(X_{cand}) + (1 - w_{cr})M_{sc} \tag{14}$$

The term $\widehat{y}_{sc}(X_{cand}) = [\widehat{\mathbf{y}}(X_{cand}) - y^{\min}] / [y^{\max} - y^{\min}]$ focuses more on the predicted optimum (exploitation) based on the constraint function calculations with the coRKG surrogates and represents the rescaled formulation of the estimated objective function values of the candidate points X_{cand}. The values $y^{\min}$ and $y^{\max}$ are the minimum and maximum values of the objective function estimates before rescaling, respectively. However, it is also desirable to improve the knowledge of the surrogates on points further from the region of the current optimum (exploration) to avoid getting stuck on local optima too quickly. That is achieved via the term M_{sc} in the merit function and here is expressed in two different versions.

The first version, defined as $M_{sc}^d = [d^{\max} - d^E] / [d^{\max} - d^{\min}]$, is the rescaled formulation of the set d^E which includes the minimum Euclidean distances of each point in the set X_{cand} from all existing points in the existing coKRG training dataset $\mathbf{X}_{HL}$, with $d^{\max}$ and $d^{\min}$ being the maximum and minimum values of d^E, respectively. The second utilizes the capability of coKRG models to return the prediction uncertainty $\widehat{s}_{g_i}(\mathbf{x})$ for the ith constraint function. For each x_{cand} of the X_{cand} set, the constraint with the maximum value $\widehat{g}_{\max} = \max\{\widehat{g}_{H,j}(x_{cand}), 0\}, j = 1, \ldots 2k$ is identified as well as its associated uncertainty prediction value $\widehat{s}_{g_{\max}}(x_{cand})$. In rescaled formulation, similar to M_{sc}^d, we now have $M_{sc}^{cu} = [cu^{\max} - cu^g] / [cu^{\max} - cu^{\min}]$ where cu^g represents the set of values $\widehat{s}_{g_{\max}}(X_{cand})$, with $cu^{\max}$ and $cu^{\min}$ being the maximum and minimum values of cu^g, respectively.

As shown in Eq. (14), the merit function also includes the choice of a weight parameter w_{cr}. The latter indicates how much weight the merit function puts on either exploitation or exploration. Various suggestions exist in the literature for determining the weight for this type of merit functions (e.g., Regis, 2011; Regis and Shoemaker, 2013; Tsoukalas et al., 2016). Here, we opt for a fixed weight $w_{cr} = 0.95$ due to the adopted scenario that the HF model is of extreme computational cost and only few runs can be utilized. In any case, the definition of w_{cr} depends on the available computational budget with the HF model and if improving the global accuracy of the surrogates is considered important for the problem at hand. Moreover, the two versions of the merit function used in AROMS ensure a certain distance among the infill points in the training dataset to avoid cases of close proximity that cause numerical issues with the construction of the coKRG surrogate models. According to the score given from Eq. (14) to all points in X_{cand} the candidate solution with the minimum value is then evaluated with the HF model and together with the calculated constraint function values are added to the coKRG training dataset. A flow diagram presentation of the AROMS algorithm as implemented for our problem is given in Fig. 3.

4. Results

Before any optimization runs with the hypothetical and the real-world VDST models, coastal aquifer flow was simulated until hydraulic head and salinity distribution reached steady-state conditions in the absence of pumping. Next, an additional simulation was employed where equally distributed and intensive pumping was applied, to represent a more realistic scenario where the coastal aquifer is already stressed to a certain extent. Those simulation outputs were used as initial conditions for the VDST models to run the optimization frameworks. The optimization runs were performed for a salinity threshold of $C^t = 0.1 kg/m^3$ and the time horizon for the pumping management plan was set to 30 years. The direct optimization based on the VDST model is denoted as EAS-HF and EAS-LF indicates the direct optimization based on the sharp interface model. To ensure a fairer comparison among the SBO methods in terms of initial conditions, 30 Latin Hypercube Sampling (LHS) designs of the LF points (the N_L set) were generated based on MATLAB's *lhsdesign* function (Statistics and Machine Learning Toolbox

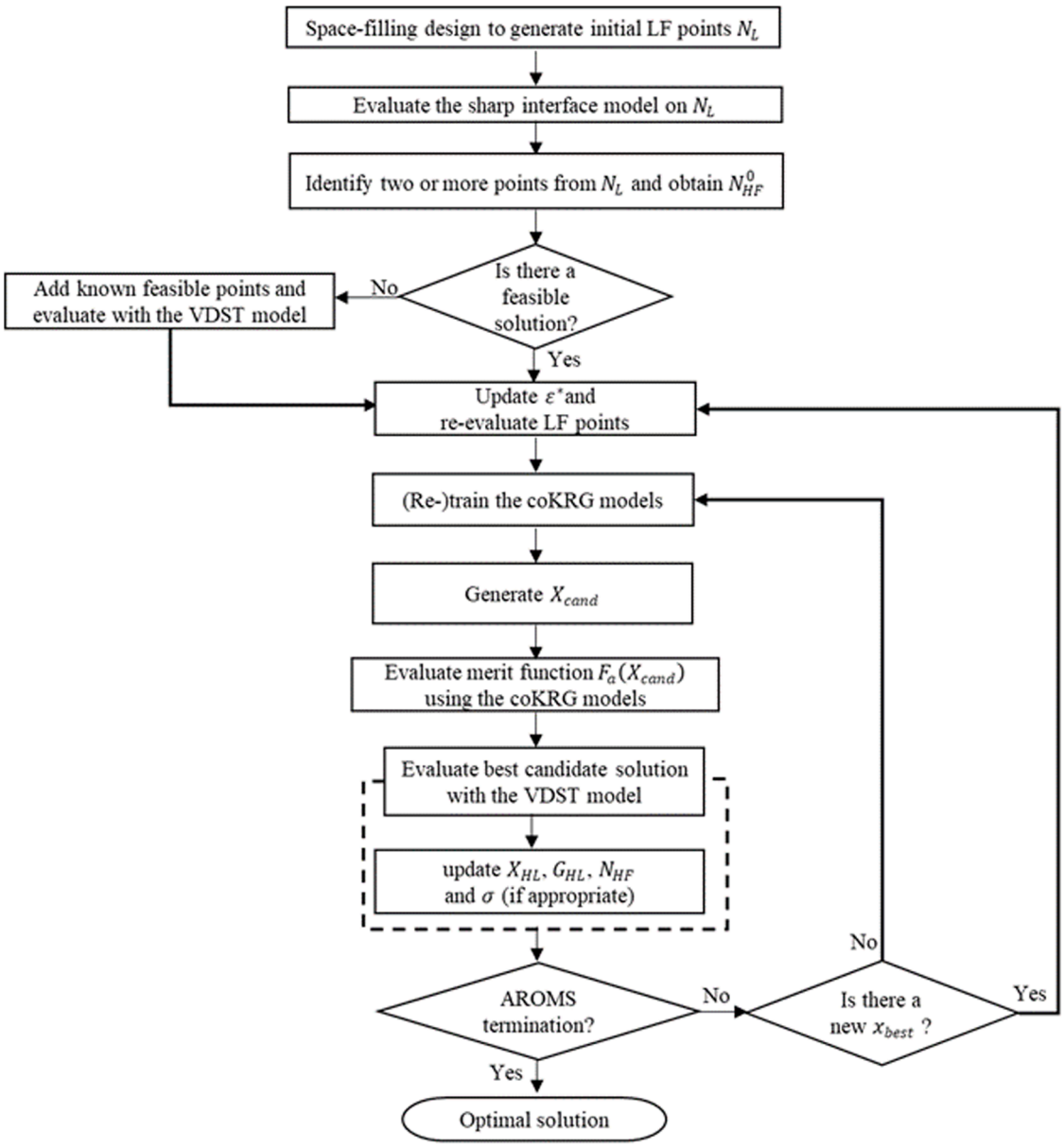

Fig. 3. Workflow diagram of AROMS algorithm using a LF sharp interface model and a HF VDST model.

2021) and were used for running the independent optimization trials with AROMS. Regarding the comparison with the single-fidelity ConstrLMSRBF algorithm two cases were examined. First, an initial independent LHS training design of $k + 1$ points was generated for the RBF models without information from the LF runs. Second, the initial LF sample points were also used for the initial training design of the ConstrLMSRBF algorithm (henceforth called ConstrLMSRBF^{LF}) by selecting a space-filling subset of $k + 1$ points by using the exchange algorithm (Forrester et al., 2007). This was in order to investigate if the larger set of points provided by the LF runs could have a notable improvement on ConstrLMSRBF algorithm performance.

For convenience, AROMS^{d} denotes the case for the distance criterion M_{sc}^{d} while AROMS^{cu} denotes the case for the uncertainty prediction criterion M_{sc}^{cu} as described previously in Eq. (14). We examine the performance of AROMS for three limited HF computational budgets of N_{max} = 22, N_{max} = 50 and N_{max} = 100. The first is in the range of $2(k + 1)$ which is commonly utilized as initial sampling size for single-fidelity SBO methods, however here it is considered as the extreme case where we can only afford a few HF simulations (k = 10 in the hypothetical problem and k = 11 in the real-world problem). We also investigate the impact of using more LF points, that is, two scenarios of $N_L = 100$ and $N_L = 200$. It is noted that the LF model used in this study is computationally cheap but overestimates the seawater intrusion extent under pumping; therefore we want to investigate if adding more LF samples offers any advantages, or it just adds computational cost to the development of the coKRG models. For all SBO comparisons, a one-way analysis of variance (ANOVA) test followed by a multiple comparison test, using the Tukey–Kramer procedure, was conducted on the best feasible objective function values to assess which method has statistically significantly better sample mean than the other, based on the p-values. The analysis was based on the built-in MATLAB functions *anova1* and *multcompare* (Statistics and Machine Learning Toolbox 2021). All simulations and optimization runs have been performed on 2.7 GHz Intel i5 processor with 8 GB of RAM in a 64-bit Windows 10 system.

4.1. Results from the hypothetical model

Here, we present the results obtained from running the optimization

Table 1
Optimal solutions from the HF VDST and LF sharp interface models along with summary of sample statistics for the SBO frameworks using 22 HF model runs and 100 LF model runs. Best values for the SBO methods are in bold and the benchmark HF near global optimum is underlined.

Optimization method	Total maximum pumping (m^3/day)				VDST model runs	Sharp interface model runs	Time*** (hr)
EAS-HF			5.1101e+03		4700	NA*	36.18
EAS-LF			3.9665e+03		NA*	7000	0.61
	Worst (m^3/day)	Best (m^3/day)	Mean (m^3/day)	Standard error (mean)	VDST model runs	Sharp interface model runs	
AROMS^{d}	4.5519e+03	4.9345e+03	4.8207e+03	15.8924	22	100	0.32
AROMS^{cu}	**4.6364e+03**	**4.9770e+03**	**4.8396e+03**	**13.3537**	22	100	0.33
ConstrLMSRBF	4.4185e+03	4.8975e+03	4.6127e+03	23.3188	22	NA*	0.16
ConstrLMSRBF^{LF}	4.3265e+03	4.8315e+03	4.6116e+03	25.4594	22	100	0.17

* Not Applicable, ** average time for the SBO methods.

problem based on the hypothetical coastal aquifer model. It is reminded that the assessment of the SBO methods was based on sample statistics from 30 independent trials. A single optimization run was conducted with the VDST and the sharp interface model with EAS, as it has previously shown a robust performance in pumping optimization problems of coastal aquifers (Christelis et al., 2019; Kopsiaftis et al., 2019). Therefore, EAS-HF and EAS-LF represent the benchmark near global optimal solutions that were obtained without any restrictions on the number of VDST and sharp interface model runs. Table 1 shows the performance of the SBO optimization methods for $N_L = 100$ and $N_{\max} = 22$ while Fig. 4 illustrates simulation outputs from both model fidelities for given pumping rates.

For this extreme scenario of only 22 HF runs, ConstrLMSRBF was not expected to be as competitive as AROMS, but it is promising that the latter clearly outperformed the former with notably better sample statistics and a p-value in the order of 10^{-12} between AROMS^{cu} and the two ConstrLMSRBF implementations. AROMS^{cu} also has better sample statistics than AROMS^{d} but the ANOVA test didn't show a statistically significant difference. All SBO methods outperform EAS-LF which provides a much lower global optimum than the corresponding EAS-HF approach. It is noteworthy that AROMS^{cu} can locate in its best run an optimal solution that is quite close to the benchmark optimum from the EAS-HF approach.

Another useful way to compare the SBO algorithms is to employ the actual relative improvement I, the maximum possible relative improvement $I_{\max}$ and the relative improvement ratio r_I metrics (Viana et al., 2010). These metrics are defined as follows:

$$I = \frac{y_{inB} - \hat{y}^*}{|y_{inB}|},\ I_{\max} = \frac{y_{inB} - y^*_{HF}}{|y_{inB}|},\ r_I = \frac{I}{I_{\max}} \tag{15}$$

where y_{inB} is the initial best solution (could be the one from the initial design points), $\hat{y}^*$is the actual solution found from the SBO algorithm and y^*_{HF} is the global optimum known from the optimization with the HF model. If $I = 0$ means that the SBO algorithm did not improve further from the known starting best feasible solution. When $I > 0$ means that there is improvement over the starting feasible solution which could be significant depending on the progress of the algorithm. Accordingly, $I_{\max}$ sets a standard of how far the initial best feasible point from the "true" global optimum is. Therefore, a ratio r_I closer to the value of 1 indicates an algorithm that produced significant progress during optimization and found a solution closer to the region of the global optimum. These measures can be used in a progress plot showing the improvement over the number of HF model runs.

From the relative improvement ratio is evident that AROMS climbs

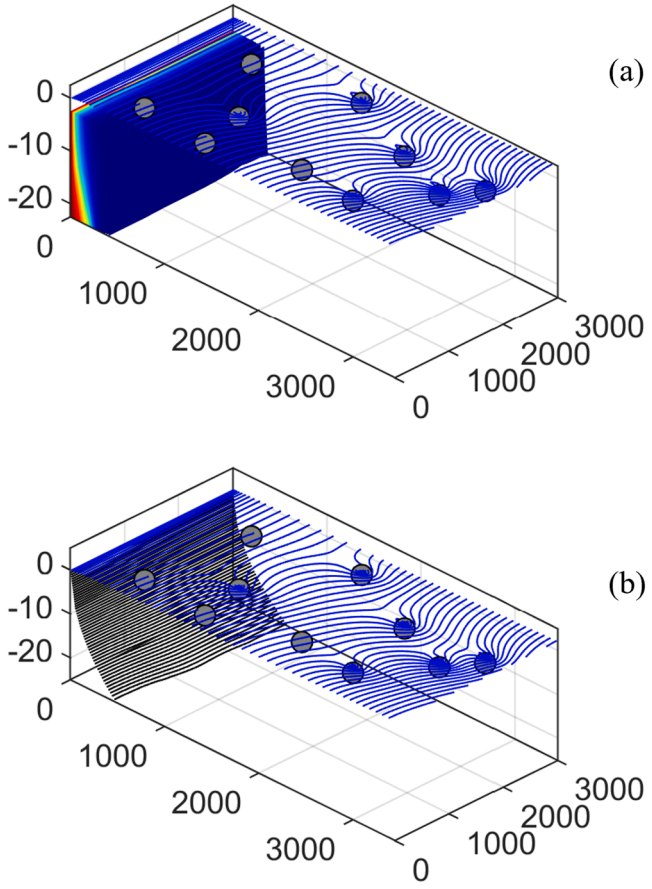

Fig. 4. Salinity and hydraulic head contours corresponding to optimal pumping rates for the VDST model (plot a) and hydraulic head and calculated interface for the same pumping rates for the sharp interface model (plot b). Results are shown for smaller part of the grid to enable a better visual comparison between the outputs of the two seawater intrusion models closer to the location of the pumping wells (grey dots).

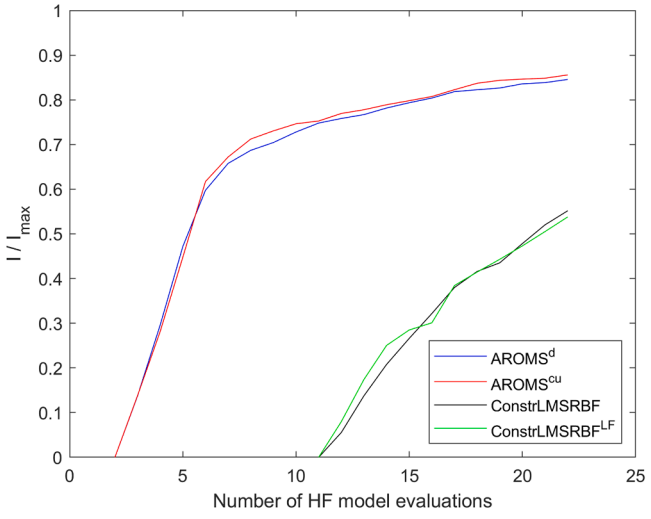

Fig. 5. Mean of the relative improvement ratio r_1 out of 30 optimization trials for $N_{\max} = 22$. Notice that plotting starts at a different number of HF points for AROMS and ConstrLMSRBF frameworks due to the different requirements for initial HF design points.

Table 2
Optimal solutions from the HF VDST and LF sharp interface models along with summary of sample statistics for the SBO frameworks using 50 HF model runs and 100 LF model runs. Best values for the SBO methods are in bold and the benchmark HF near global optimum is underlined.

Optimization method	Total maximum pumping (m^3/day)				VDST model runs	Sharp interface model runs	Time*** (hr)
EAS-HF			5.1101e+03		4700	NA*	36.18
EAS-LF			3.9665e+03		NA*	7000	0.61
	Worst (m^3/day)	Best (m^3/day)	Mean (m^3/day)	Standard error (mean)	VDST model runs	Sharp interface model runs	
AROMS^{d}	**4.7942e+03**	4.9773e+03	4.8869e+03	**10.4816**	50	100	0.67
AROMS^{cu}	4.7861e+03	**5.0520e+03**	**4.9232e+03**	10.9812	50	100	0.68
ConstrLMSRBF	4.5281e+03	4.9454e+03	4.8582e+03	13.5015	50	NA*	0.33
ConstrLMSRBF^{LF}	4.7715e+03	5.0202e+03	4.8741e+03	10.8416	50	100	0.34

* Not Applicable, ** average time for the SBO methods.

fast to a value of $r_1 = 0.8$ in about 18 HF model runs (Fig. 5), which is a promising performance that justifies AROMS application to optimization problems of quite small HF training datasets. On the other hand, ConstrLMSRBF stays on much lower r_1 values but shows a marked potential of improvement given that more HF points can be added. As AROMS borrows the main sampling strategy from ConstrLMSRBF it is indicative that such an approach binds well with coKRG surrogate models and offers a computationally efficient method to deal with pumping optimization problems of certain type.

Table 2 and Fig. 6 present the results for $N_L = 100$ and $N_{max} = 50$. As expected, the addition of more HF infill points improved the performance of all SBO methods with mean values even closer to the benchmark global optimum. Again, AROMS^{cu} appears to outperform the other frameworks with a p-value in the order of 10^{-4} against standard ConstrLMSRBF and 10^{-3} against ConstrLMSRBF^{LF}. There was no statistically significant difference between AROMS^{d} and AROMS^{cu} and neither between ConstrLMSRBF and ConstrLMSRBF^{LF}, but this time the latter provided better sample statistics, which might indicate that the information from the LF runs is useful for improving ConstrLMSRBF when more HF points are available. Also, this time there was no statistically significant difference among AROMS^{d}, ConstrLMSRBF and ConstrLMSRBF^{LF}, which implies that the prediction uncertainty option might be more suitable for the AROMS implementation as it improves its performance. In terms of the relative improvement ratio, the performance of the multi-fidelity SBO methods approaches a value of $r_1 = 0.9$ while for the single-fidelity ConstrLMSRBF and ConstrLMSRBF^{LF} is now close to $r_1 = 0.8$ as the HF computational budget of $N_{max} = 50$ is exhausted. It should be noted here that while ConstrLMSRBF takes half the average time to run than the multi-fidelity approach, for a real-world VDST model that might run for hours this difference becomes insignificant. In other words, the higher the computational cost for a single run of the HF model the larger the benefit from the multi-fidelity approach given its strong performance, particularly regarding AROMS^{cu} framework.

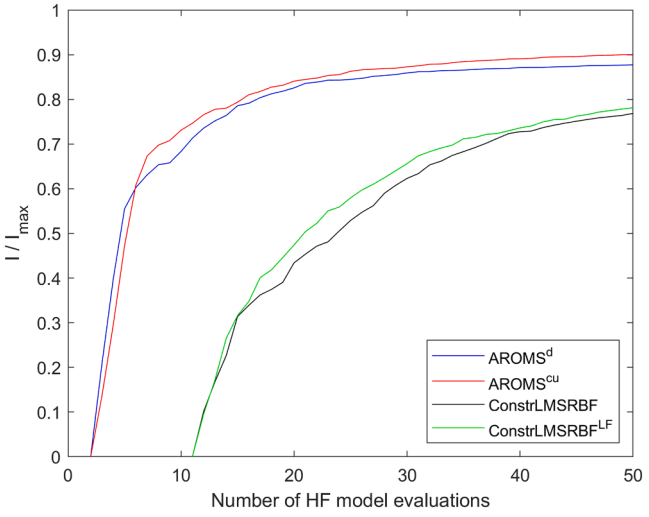

Fig. 6. Mean of the relative improvement ratio r_1 out of 30 optimization trials for $N_{max} = 50$. Notice that plotting starts at a different number of HF points for AROMS and ConstrLMSRBF frameworks due to the different requirements for initial HF design points.

It is interesting to compare the performance of AROMS^{cu} and ConstrLMSRBF^{LF} for $N_{max} = 100$, which represents, as an empirical rule of $N_{max} = 10k$, a reasonable training size of HF points in SBO applications (Jones et al., 1998). Of course, this empirical rule might be prohibitive when $k \gg 10$ (it is reminded that $k = 10$ for our hypothetical model) and the HF model is extremely time-consuming. As shown in Table 3 and Fig. 7, the multi-fidelity AROMS^{cu} framework still outperforms ConstrLMSRBF^{LF} and their sample means are statistically significantly different with a p-value of 0.0051 while at the end of 100 HF simulations the mean relative improvement ratio is $r_1 = 0.96$ for AROMS^{cu} and $r_1 = 0.83$ for ConstrLMSRBF^{LF}. Those results are particularly promising for the performance of AROMS^{cu} showing global search capabilities on a rather small total HF computational budget which is the order of $N_{max} = 10k$, at least for the case study examined here. Therefore, with a computational gain of almost 95% compared to the global search with the EAS_HF approach, AROMS^{cu} already provided an efficient and effective method to approximate the benchmark optimum using only 100 HF and 100 LF model runs.

Table 3
Optimal solutions from the HF VDST and LF sharp interface models along with summary of sample statistics for the SBO frameworks using 100 HF model runs and 100 LF model runs. Best values for the SBO methods are in bold and the benchmark HF near global optimum is underlined.

Optimization method	Total maximum pumping (m^3/day)				VDST model runs	Sharp interface model runs	Time*** (hr)
EAS-HF			5.1101e+03		4700	NA*	36.18
EAS-LF			3.9665e+03		NA*	7000	0.61
	Worst (m^3/day)	Best (m^3/day)	Mean (m^3/day)	Standard error (mean)	VDST model runs	Sharp interface model runs	
AROMS^{cu}	5.0147e+03	**5.0952e+03**	**5.0325+03**	6.3525	100	100	1.56
ConstrLMSRBF^{LF}	4.8557e+03	5.0171e+03	4.9333e+03	8.9628	100	100	0.8

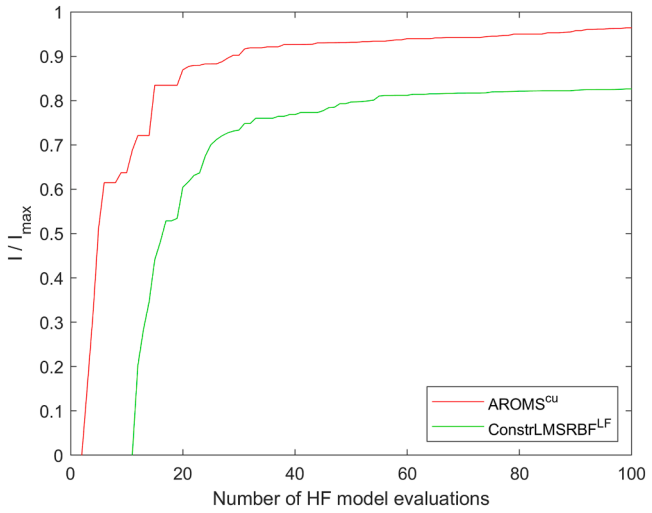

Fig. 7. Mean of the relative improvement ratio r_1 out of 30 optimization trials for $N_{\max} = 100$. Notice that plotting starts at a different number of HF points for AROMS and ConstrLMSRBF frameworks due to the different requirements for initial HF design points.

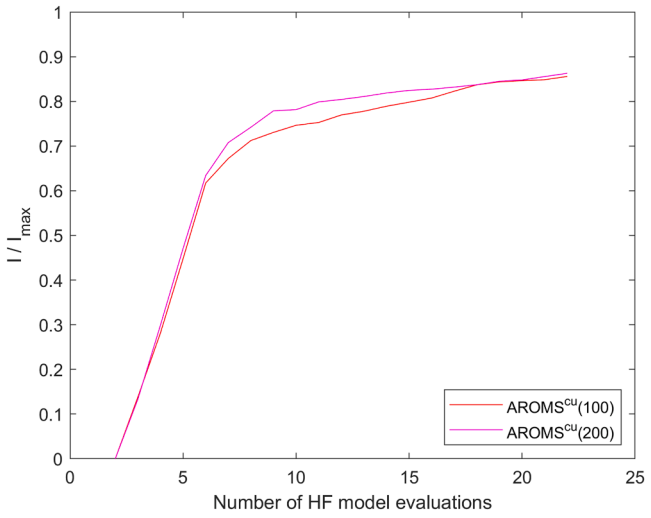

Fig. 8. Mean of the relative improvement ratio r_1 out of 30 optimization trials for two implementations of the AROMS^{cu} framework. That is,$N_L = 100$ (AROMS$^{cu\ (100)}$) and $N_L = 200$ (AROMS$^{cu\ (200)}$) while$N_{\max} = 22$.

As a last case for comparison, based on the hypothetical VDST model, we investigated the impact of adding more LF points to the AROMS^{cu} framework (Table 4 and Fig. 8). Therefore, we compare the multi-fidelity framework performance for $N_L = 100$ and $N_L = 200$ for the extreme scenario of only 22 HF model runs. While the ANOVA test returned a p-value of 0.088 indicating that the sample means do not show a statistically significant difference it is also evident that using additional LF points has improved the sample statistics of AROMS^{cu}. However, the computational cost of implementing AROMS^{cu} with 200 LF points is now higher due to the construction of coKRG surrogate models for the constraint functions based also on a larger LF sample. It is reminded that the implementation of AROMS in this study is based on a LF sharp interface model which is computationally cheap but might not correlate well with the VDST model, particularly for larger pumping rates. Therefore the benefit of adding more LF points in some cases might be less significant.

4.2. Results from the real -world model

Figure 9 presents the 3D visualization of the salinity front based on the application of the optimal pumping rates calculated with EAS-HF while Table 5 summarizes the results from the various optimization frameworks. It is noted that for the real-world case a single run was conducted for the SBO methods to test their applicability in a more realistic scenario where more trials might add undesired computational burden. Interestingly, AROMS^{cu} using only 24 HF runs and 100 LF runs at a computational cost of 1.3 h, provided an optimal solution which approximates well the global optimum found by EAS-HF. The latter converged to the optimal solution approximately after 15 days. This is a very promising result for the multi-fidelity method developed in this work and demonstrates AROMS potential to dramatically reduce the computational burden and identify very good solutions within restricted computational budgets.

Table 4
Optimal solutions from the HF VDST and LF sharp interface models along with summary of sample statistics for the SBO frameworks using 22 HF model runs and two cases for AROMS. One with 100 LF and the other with 200 LF model runs, respectively. Best values for the SBO methods are in bold and the benchmark HF near global optimum is underlined.

Optimization method	Total maximum pumping (m^3/day)				VDST model runs	Sharp interface model runs	Time*** (hr)
EAS-HF			<u>5.1101e+03</u>		4700	NA*	36.18
EAS-LF			3.9665e+03		NA*	7000	0.61
	Worst (m^3/day)	Best (m^3/day)	Mean (m^3/day)	Standard error (mean)	VDST model runs	Sharp interface model runs	
AROMS$^{cu\ (100)}$	4.6364e+03	4.9770e+03	4.8396e+03	13.3537	22	100	0.33
AROMS$^{cu\ (200)}$	**4.6933e+03**	**4.9894e+03**	**4.8703e+03**	**11.6034**	22	200	0.76

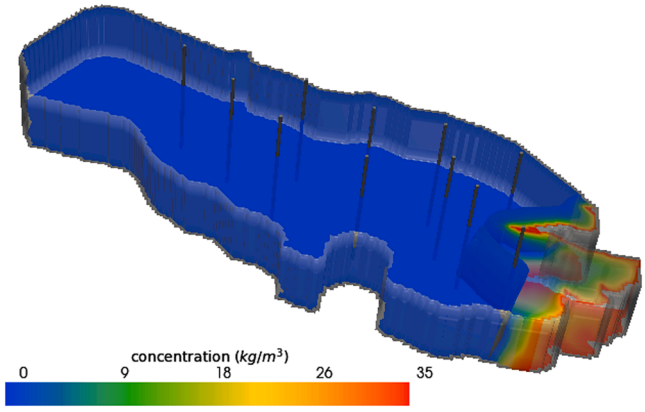

Fig. 9. Salinity distribution for the Vathi Aquifer of Kalymnos Island based on the optimal pumping rates obtained from EAS-HF. The imposed constraints keep the salinity front mostly seaward and the salinity threshold of $C^t = 0.1kg/m^3$ marginally reaches but does not intersect the three pumping wells which are closer to the coast.

Table 5
Optimal solutions for the real-world optimization problem. Best values for the SBO methods are in bold and the benchmark HF near global optimum is underlined.

Optimization method	Total maximum pumping (m^3/day)	VDST model runs	Sharp interface model runs	Time*** (hr)
EAS-HF	7.4869e+03	8800	NA*	367
EAS-LF	5.8288e+03	NA*	5774	2.52
ConstrLMSRBF	6.9758e+03	24	NA	1.09
AROMS^{cu}	**7.3870e+03**	24	100	1.30

As the results from both SBO methods show a very good performance with a very small HF training sample, we further discuss the specifications related to this real-world example. Based on our previous experience with this specific coastal aquifer model, there are some unique features related to the optimization problem defined here. The shape of the coastline, the geographical location of the pumping wells and the strict constraint functions, which include both salinity and hydraulic heads, do not allow abrupt inland movement of the salinity front even for larger pumping rates. This situation holds for both direct optimization frameworks, that is, using the VDST or the sharp interface model alone. As a result, the constraints related to salinity (or interface toe for the LF case), which inherently present a stronger non-linear response to pumping compared to the hydraulic head constraints, are less active during optimization. Therefore, the constraints related to hydraulic heads are those that mainly determine the feasibility of the candidate solutions. This specific condition facilitates the notable improvement of the surrogate models of the constraint functions in the region of the current best solution without the requirement for large HF training samples. In other words, it is an easier task for the SBO frameworks given that the stronger non-linear constraints have a smoother response which also explains the good performance of the ConstrLMSRBF algorithm based on only 24 HF simulations. Therefore, the results obtained for the Vathi aquifer in Kalymnos Island, demonstrate that AROMS and ConstrLMSRBF frameworks, which share a similar sampling strategy, are capable of a steep improvement of the objective function within very limited HF computational budgets for an optimization problem with less non-linear constraints. It is noted that this is not the case for the hypothetical coastal aquifer model where the salinity constraints are the ones that determine the feasibility of solutions which shows the capability of AROMS to approximate the HF optimum under more challenging optimization settings.

5. Discussion

Results showed that the proposed multi-fidelity framework has the potential to address satisfactorily pumping optimization problems in coastal aquifer management that involve only a small number of runs with the VDST models. AROMS approximated well the HF optimal solutions and outperformed the corresponding single-fidelity approach. Nevertheless, there are a few points that are worthy of further discussion.

One point pertains to the selection of the surrogate models for running the SBO frameworks. Regarding the comparisons with the single-fidelity ConstrLMSRBF algorithm, it could be argued that its performance might be improved if instead of RBF models the framework would be implemented based on Kriging models for the constraint functions. In that case, a similar merit function to AROMS can be derived which utilizes the uncertainty prediction capabilities of Kriging surrogate models. However, this is mainly a hypothesis as previous studies in water resources optimization have shown that more complex surrogate models do not necessarily ensure a better performance for a single-fidelity SBO framework (e.g., Babaei and Pan, 2016; Christelis et al., 2019). Here, given the previous robust performance of ConstrLMSRBF on similar problems (Christelis et al., 2018), it was considered as a baseline method to compare with AROMS which also utilizes a similar sampling strategy. Future studies might further explore the capabilities of these two SBO frameworks using different selection of surrogate modelling techniques either for single- or multi-fidelity implementations. It is noted that the present study is, to the best of our knowledge, the first that examines in detail multi-fidelity optimization schemes that balance exploration with exploitation under restricted HF computational budgets for coastal aquifer management.

Another point of interest is the selection of an appropriate LF model for implementing AROMS framework. Further studies should focus on the impact of using more accurate LF models and what is their impact on the overall computational cost. In general, other computationally faster approaches that better approximate the response of VDST models (e.g., Mazi and Koussis 2021; Coulon et al., 2022; Park et al., 2023) should improve the performance of AROMS, but it remains to be seen if the enhanced accuracy justifies the anticipated increase in the computational cost for running the multi-fidelity framework. It is noted that the optimization problems tested here involved about 20 constraint functions and a moderate number of decision variables (10 for the hypothetical and 11 for the real-world case). Whether it is beneficial to use AROMS for larger dimensionalities and many constraint functions should be further investigated given the computational complexity and cost of coKRG models. It might be the case that other approaches of building multi-fidelity surrogates are a better choice for different problem settings. A more challenging situation is also to examine multi-fidelity optimization methods on transient pumping stresses and/or recharge variations, but thus far this largely remains an unexplored research area in coastal aquifer management even for single-fidelity SBO methods. Also, it should be noted that at this stage the AROMS framework has been developed on the basis that a deterministic simulation of seawater intrusion is sufficient for calculating optimal pumping rates. Thus, the uncertainty in the prediction of seawater intrusion extent is not considered and this is an aspect that could be further explored in future implementations of AROMS.

In overall, AROMS framework appears to have a consistent performance and can be easily tailored to the needs of different formulations of the optimization problem while it can be adjusted according to the type of the LF model that is employed for the problem at hand. Based on preliminary runs with AROMS, which were not shown here for brevity, the choice of the initial HF points for building the coKRG models has a significant role on its performance. As the method focuses on quite small number of runs with the HF model, the inclusion of feasible HF points at the beginning is essential, particularly if the LF model strongly deviates from the response of the HF model for various sets of pumping rates.

Here, we aim to overcome this problem through the adaptive correction of the buoyancy ratio but different model parametrizations, boundary conditions or coastal aquifer flow conceptualizations might also require a different handling.

6. Conclusions

The high runtime of a VDST numerical model might be computationally prohibitive to solve pumping optimization problems of coastal aquifers. In some cases, the computational cost might also hinder the implementation of SBO methods that rely on single-fidelity surrogate models. To address this case, we proposed a multi-fidelity SBO framework which utilizes co-Kriging surrogate models and multiple simulations from LF sharp interface models. The multi-fidelity SBO method, called AROMS, successfully locates good local optima using only a few VDST model runs with substantial savings in the computational cost. The proposed method demonstrated a competitive performance to also locate solutions near the global optimum when larger HF training datasets were utilized, and it outperformed a corresponding single-fidelity SBO method.

This is, to the best of our knowledge, the first work to develop a multi-fidelity optimization scheme for costal aquifer management that balances exploration with exploitation for restricted computational budgets. The promising performance of the proposed method implies that it could be potentially used for other groundwater management problems by modifying it accordingly. We anticipate that the method developed in this work can offer a useful computational tool for real-world pumping optimization problems with complex and computationally expensive VDST models. Furthermore, we believe that the promising results of the present work highlight the need for additional research on multi-fidelity optimization for coastal aquifer management to confront the computational challenges associated with complex VDST models. Future work would seek to explore the incorporation of other lower fidelity models of seawater intrusion for transient flow stresses and pumping and investigate the capabilities of the proposed methodology for high-dimensional optimization problems.

CRediT authorship contribution statement

Vasileios Christelis: Conceptualization, Methodology, Software, Formal analysis, Writing – original draft. **George Kopsiaftis:** Conceptualization, Methodology, Software, Writing – review & editing. **Rommel G. Regis:** Methodology, Software, Supervision, Writing – review & editing. **Aristotelis Mantoglou:** Conceptualization, Methodology, Supervision, Writing – review & editing.

Declaration of Competing Interest

The authors declare that they have no known competing financial interests or personal relationships that could have appeared to influence the work reported in this paper.

Data availability

Data will be made available on request.

Acknowledgments

Preliminary results of the present work have been orally presented in XXIV International Conference on Computational Methods in Water Resources (CMWR) that was held at the Gdańsk University of Technology, 19–23 June 2022. VC publishes with permission of the Director, British Geological Survey. The authors would like to thank the two reviewers, Dr. Antonis Koussis and one anonymous, for their time to provide insightful comments and constructive critique that enabled the improvement of the submitted manuscript.

References

Ataie-Ashtiani, B., Ketabchi, H., Rajabi, M.M., 2014. Optimal management of a freshwater lens in a small island using surrogate models and evolutionary algorithms. J. Hydrol. Eng. 19, 339–354.

Babaei, M., Pan, I., 2016. Performance comparison of several response surface surrogate models and ensemble methods for water injection optimization under uncertainty. Comput. Geosci. 91, 19–32. https://doi.org/10.1016/j.cageo.2016.02.022.

Bakker, M., Oude Essink, G.H.P., Langevin, C.D., 2004. The rotating movement of three immiscible fluids—a benchmark problem. J. Hydrol. 287, 270–278. https://doi.org/10.1016/j.jhydrol.2003.10.007.

Bakker, M., 2003. A Dupuit formulation for modeling seawater intrusion in regional aquifer systems. Water Resour. Res. 39 https://doi.org/10.1029/2002WR001710.

Bandler, J.W., Cheng, Q.S., Nikolova, N.K., Ismail, M.A., 2004. Implicit space mapping optimization exploiting preassigned parameters. IEEE Trans. Microw. Theory Tech. 52, 378–385.

Bianchi, M., Zheng, L., Birkholzer, J.T., 2016. Combining multiple lower-fidelity models for emulating complex model responses for CCS environmental risk assessment. Int. J. Greenhouse Gas Control 46, 248–258. https://doi.org/10.1016/j.ijggc.2016.01.009.

Bomers, A., Schielen, R.M.J., Hulscher, S.J.M.H., 2019. Application of a lower-fidelity surrogate hydraulic model for historic flood reconstruction. Environ. Model. Softw. 117, 223–236. https://doi.org/10.1016/j.envsoft.2019.03.019.

Castelletti, A., Galelli, S., Restelli, M., Soncini-Sessa, R., 2012. Data-driven dynamic emulation modelling for the optimal management of environmental systems. Environ. Model. Softw. 34, 30–43. https://doi.org/10.1016/j.envsoft.2011.09.003.

Cheng, J., Lin, Q., Yi, J., 2022. An enhanced variable-fidelity optimization approach for constrained optimization problems and its parallelization. Struct. Multidisc. Optim. 65, 188. https://doi.org/10.1007/s00158-022-03283-0.

Christelis, V., Hughes, A.G., 2022. Multifidelity surrogate models for efficient uncertainty propagation analysis in salars systems. Front. Water 4. https://doi.org/10.3389/frwa.2022.827036.

Christelis, V., Mantoglou, A., 2016. Coastal aquifer management based on the joint use of density-dependent and sharp interface models. Water Resour. Manage. 30, 861–876. https://doi.org/10.1007/s11269-015-1195-4.

Christelis, V., Mantoglou, A., 2019. Pumping optimization of coastal aquifers using seawater intrusion models of variable-fidelity and evolutionary algorithms. Water Resour. Manage. 33, 555–568. https://doi.org/10.1007/s11269-018-2116-0.

Christelis, V., Regis, R.G., Mantoglou, A., 2018. Surrogate-based pumping optimization of coastal aquifers under limited computational budgets. J. Hydroinf. 20, 164–176. https://doi.org/10.2166/hydro.2017.063.

Christelis, V., Kopsiaftis, G., Mantoglou, A., 2019. Performance comparison of multiple and single surrogate models for pumping optimization of coastal aquifers. Hydrol. Sci. J. 64, 336–349. https://doi.org/10.1080/02626667.2019.1584400.

Christelis, V., 2021. PhD Thesis.

Couckuyt, I., Dhaene, T., Demeester, P., 2014. ooDACE toolbox: a flexible object-oriented Kriging implementation. J. Mach. Learn Res. 15, 3183–3186.

Coulon, C., Lemieux, J.M., Pryet, A., Bayer, P., Young, N.L., Molson, J., 2022. Pumping optimization under uncertainty in an island freshwater lens using a sharp-interface seawater intrusion model. Water Resour. Res. 58 (8), e2021WR031793.

Dausman, A.M., Langevin, C., Bakker, M., Schaars, F., 2010. A comparison between SWI and SEAWAT – the importance of dispersion, inversion and vertical anisotropy.

Dey, S., Prakash, O., 2020. Managing saltwater intrusion using conjugate sharp interface and density dependent models linked with pumping optimization. Groundw. Sustain. Develop. 11, 100446 https://doi.org/10.1016/j.gsd.2020.100446.

Durantin, C., Rouxel, J., Désidéri, J.-A., Glière, A., 2017. Multifidelity surrogate modeling based on radial basis functions. Struct. Multidisc. Optim. 56, 1061–1075. https://doi.org/10.1007/s00158-017-1703-7.

Efstratiadis, A., Koutsoyiannis, D., 2002. An evolutionary annealing-simplex algorithm for global optimisation of water resource systems. In: Proceedings of the fifth international conference on hydroinformatics, 11. International Water Association, Cardiff, UK, pp. 431–441.

Fernández-Godino, G., Park, M., Kim, C., Haftka, N.H., 2019. Issues in deciding whether to use multifidelity surrogates. AIAA J. 57, 2039–2054. https://doi.org/10.2514/1.J057750,https://doi.org/10.1615/Int.J.UncertaintyQuantification.2014006914.

Forrester, A.I.J., Keane, A.J., 2009. Recent advances in surrogate-based optimization. Prog. Aerosp. Sci. 45, 50–79. https://doi.org/10.1016/j.paerosci.2008.11.001.

Forrester, A.I.J., Sóbester, A., Keane, A.J., 2007. Multi-fidelity optimization via surrogate modelling. Proceed. Roy. Soc. A: Math. Phys. Eng. Sci. 463, 3251–3269. https://doi.org/10.1098/rspa.2007.1900.

Forrester, A.I.J., Sóbester, A., Keane, A.J., 2008. Engineering Design Via Surrogate Modelling – A Practical Guide. Wiley, New York.

Gano, S., Sanders, B., Renaud, J., 2004. Variable fidelity optimization using a Kriging based scaling function. In: 10th AIAA/ISSMO Multidisciplinary Analysis and Optimization Conference. American Institute of Aeronautics and Astronautics, Albany, New York. https://doi.org/10.2514/6.2004-4460.

Hamzehloo, A., Bahlali, M.L., Salinas, P., Jacquemyn, C., Pain, C.C., Butler, A.P., Jackson, M.D., 2022. Modelling saline intrusion using dynamic mesh optimization with parallel processing. Adv. Water Res. 164, 104189 https://doi.org/10.1016/j.advwatres.2022.104189.

Jiao, R., Zeng, S., Li, C., Jiang, Y., Jin, Y., 2019. A complete expected improvement criterion for Gaussian process assisted highly constrained expensive optimization. Inform. Sci. 471, 80–96. https://doi.org/10.1016/j.ins.2018.09.003.

Jones, D.R., Schonlau, M., Welch, W.J., 1998. Efficient global optimization of expensive black-box functions. J. Glob. Optim. 13, 455–492. https://doi.org/10.1023/A:1008306431147.
Ketabchi, H., Ataie-Ashtiani, B., 2015. Assessment of a parallel evolutionary optimization approach for efficient management of coastal aquifers. Environ. Model. Softw. 74, 21–38. https://doi.org/10.1016/j.envsoft.2015.09.002.
Kopsiaftis, G., Christelis, V., Mantoglou, A., 2019. Comparison of sharp interface to variable density models in pumping optimisation of coastal aquifers. Water Resour. Manage. 33, 1397–1409. https://doi.org/10.1007/s11269-019-2194-7.
Koussis, A.D., Mazi, K., Destouni, G., 2012. Analytical single-potential, sharp-interface solutions for regional seawater intrusion in sloping unconfined coastal aquifers, with pumping and recharge. J. Hydrol. 416–417, 1–11. https://doi.org/10.1016/j.jhydrol.2011.11.012.
Koussis, A.D., Mazi, K., Riou, F., Destouni, G., 2015. A correction for Dupuit–Forchheimer interface flow models of seawater intrusion in unconfined coastal aquifers. J. Hydrol. 525, 277–285. https://doi.org/10.1016/j.jhydrol.2015.03.047.
Koziel, S., Leifsson, L., 2016. Simulation-driven Design By Knowledge-Based Response Correction Techniques. Springer.
Koziel, S., Leifsson, L., Couckuyt, I., Dhaene, T., 2013. Robust variable-fidelity optimization of microwave filters using co-Kriging and trust regions. Microw. Opt. Technol. Lett. 55, 765–769. https://doi.org/10.1002/mop.27447.
Kreitmair, M.J., Makasis, N., Menberg, K., Bidarmaghz, A., Farr, G.J., Boon, D.P., Choudhary, R., 2022. Bayesian parameter inference for shallow subsurface modeling using field data and impacts on geothermal planning. Data-Centr. Eng. 3, e32. https://doi.org/10.1017/dce.2022.32.
Lal, A., Datta, B., 2018. Development and implementation of support vector machine regression surrogate models for predicting groundwater pumping-induced saltwater intrusion into coastal aquifers. Water Resour. Manage. 32, 2405–2419. https://doi.org/10.1007/s11269-018-1936-2.
Langevin, C.D., Guo, W., 2006. MODFLOW/MT3DMS-based simulation of variable-density ground water flow and transport. Ground Water 44, 339–351. https://doi.org/10.1111/j.1745-6584.2005.00156.x.
Le Gratiet, L., Garnier, J., 2014. Recursive co-Kriging model for design of computer experiments with multiple levels of fidelity. Int. J. Uncert. Quantif. 4 (5).
Lim, T.C., 2021. Model emulators and complexity management at the environmental science-action interface. Environ. Model. Softw. 135, 104928 https://doi.org/10.1016/j.envsoft.2020.104928.
Liu, B., Koziel, S., Zhang, Q., 2016. A multi-fidelity surrogate-model-assisted evolutionary algorithm for computationally expensive optimization problems. J. Comput. Sci. 12, 28–37. https://doi.org/10.1016/j.jocs.2015.11.004.
Lu, W., Xia, W., Shoemaker, C.A., 2022. Surrogate global optimization for identifying cost-effective green infrastructure for urban flood control with a computationally expensive inundation model. Water Resour. Res. 58, e2021WR030928 https://doi.org/10.1029/2021WR030928.
Man, J., Lin, G., Yao, Y., Zeng, L., 2021. A generalized multi-fidelity simulation method using sparse polynomial chaos expansion. J. Comput. Appl. Math. 397, 113613 https://doi.org/10.1016/j.cam.2021.113613.
Mantoglou, A., Papantoniou, M., Giannoulopoulos, P., 2004. Management of coastal aquifers based on nonlinear optimization and evolutionary algorithms. J. Hydrol. 297, 209–228. https://doi.org/10.1016/j.jhydrol.2004.04.011.
Mantoglou, A., 2003. Pumping management of coastal aquifers using analytical models of saltwater intrusion. Water Resour. Res. 39 https://doi.org/10.1029/2002WR001891.
Mazi, K., Koussis, A.D., 2021. Beyond pseudo-coupling: computing seawater intrusion in coastal aquifers with decoupled flow and transport equations. J. Hydrol. 593, 125794.
Menberg, K., Bidarmaghz, A., Gregory, A., Choudhary, R., Girolami, M., 2020. Multi-fidelity approach to Bayesian parameter estimation in subsurface heat and fluid transport models. Sci. Total Environ. 745, 140846 https://doi.org/10.1016/j.scitotenv.2020.140846.
Moreno-Rodenas, A.M., Bellos, V., Langeveld, J.G., Clemens, F.H.L.R., 2018. A dynamic emulator for physically based flow simulators under varying rainfall and parametric conditions. Water Res. 142, 512–527. https://doi.org/10.1016/j.watres.2018.06.011.
Müller, J., Woodbury, J.D., 2017. GOSAC: global optimization with surrogate approximation of constraints. J. Glob. Optim. 69, 117–136. https://doi.org/10.1007/s10898-017-0496-y.
Nagkoulis, N., Katsifarakis, K.L., 2022. Using game theory to assign groundwater pumping schedules. Water Resour. Manag. 36, 1571–1586.
Pang, M., Du, E., Shoemaker, C.A., Zheng, C., 2022. Efficient, parallelized global optimization of groundwater pumping in a regional aquifer with land subsidence constraints. J. Environ. Manage. 310, 114753 https://doi.org/10.1016/j.jenvman.2022.114753.
Park, Y.J., Hwang, H.T., Hasegawa, T., Okamoto, S., Ozutsumi, T., Tanaka, T., Morita, Y., Illman, W.A., 2023. Steady-state density-driven flow and transport: pseudo-transient parameter continuation. Adv. Water Res., 104380 https://doi.org/10.1016/j.advwatres.2023.104380.
Pellegrini, R., Serani, A., Diez, M., Wackers, J., Queutey, P., Visonneau, M., 2018. Adaptive sampling criteria for multi-fidelity metamodels in CFD-based shape optimization. In ECCOMAS CFD 2018.
Perdikaris, P., Venturi, D., Royset, J.O., Karniadakis, G.E., 2015. Multi-fidelity modelling via recursive co-Kriging and Gaussian–Markov random fields. Proc. R. Soc. A. 471, 20150018 https://doi.org/10.1098/rspa.2015.0018.
Perdikaris, P., Raissi, M., Damianou, A., Lawrence, N.D., Karniadakis, G.E., 2017. Nonlinear information fusion algorithms for data-efficient multi-fidelity modelling. Proceed. Roy. Soc. A: Math. Phys. Eng. Sci. 473, 20160751 https://doi.org/10.1098/rspa.2016.0751.
Pool, M., Carrera, J., 2011. A correction factor to account for mixing in Ghyben-Herzberg and critical pumping rate approximations of seawater intrusion in coastal aquifers. Water Resour. Res. 47 https://doi.org/10.1029/2010WR010256.
Razavi, S., Tolson, B.A., Burn, D.H., 2012. Review of surrogate modeling in water resources. Water Resour. Res. 48 https://doi.org/10.1029/2011WR011527.
Regis, R.G., Shoemaker, C.A., 2005. Constrained global optimization of expensive black box functions using radial basis functions. J. Glob. Optim. 31, 153–171. https://doi.org/10.1007/s10898-004-0570-0.
Regis, R.G., Shoemaker, C.A., 2013. Combining radial basis function surrogates and dynamic coordinate search in high-dimensional expensive black-box optimization. Eng. Optim. 45, 529–555. https://doi.org/10.1080/0305215X.2012.687731.
Regis, R.G., 2011. Stochastic radial basis function algorithms for large-scale optimization involving expensive black-box objective and constraint functions. Comput. Opera. Res. 38, 837–853. https://doi.org/10.1016/j.cor.2010.09.013.
Regis, R.G., 2014a. Constrained optimization by radial basis function interpolation for high-dimensional expensive black-box problems with infeasible initial points. Eng. Optim. 46, 218–243. https://doi.org/10.1080/0305215X.2013.765000.
Regis, R.G., 2014b. Evolutionary programming for high-dimensional constrained expensive black-box optimization using radial basis functions. IEEE Trans. Evol. Computat. 18, 326–347. https://doi.org/10.1109/TEVC.2013.2262111.
Robinson, T., Willcox, K., Eldred, M., Haimes, R., 2006. Multifidelity optimization for variable-complexity design. In: 11th AIAA/ISSMO Multidisciplinary Analysis and Optimization Conference. Presented at the 11th AIAA/ISSMO Multidisciplinary Analysis and Optimization Conference. American Institute of Aeronautics and Astronautics, Portsmouth, Virginia. https://doi.org/10.2514/6.2006-7114.
Roy, D.K., Datta, B., 2019. Adaptive management of coastal aquifers using entropy-set pair analysis–based three-dimensional sequential monitoring network design. J. Hydrol. Eng. 24, 04018072 https://doi.org/10.1061/(ASCE)HE.1943-5584.0001765.
Rozos, E., Mazi, K., Koussis, A.D., 2021. Efficient stochastic simulation of seawater intrusion, with mixing, in confined coastal aquifers. Front. Water 3, 98. https://doi.org/10.3389/frwa.2021.720557.
Ruan, X., Jiang, P., Zhou, Q., Hu, J., Shu, L., 2020. Variable-fidelity probability of improvement method for efficient global optimization of expensive black-box problems. Struct. Multidisc. Optim. 62, 3021–3052. https://doi.org/10.1007/s00158-020-02646-9.
Serani, A., Pellegrini, R., Wackers, J., Jeanson, C.-E., Queutey, P., Visonneau, M., Diez, M., 2019. Adaptive multi-fidelity sampling for CFD-based optimisation via radial basis function metamodels. Int. J. Comput. Fluid Dyn. 33, 237–255. https://doi.org/10.1080/10618562.2019.1683164.
Shi, R., Liu, L., Long, T., Wu, Y., Gary Wang, G., 2020. Multi-fidelity modeling and adaptive co-Kriging-based optimization for all-electric geostationary orbit satellite systems. J. Mech. Des. 142, 021404 https://doi.org/10.1115/1.4044321.
Siade, A.J., Cui, T., Karelse, R.N., Hampton, C., 2020. Reduced-dimensional Gaussian process machine learning for groundwater allocation planning using swarm theory. Water Resour. Res. 56, e2019WR026061 https://doi.org/10.1029/2019WR026061.
Singh, P., Couckuyt, I., Elsayed, K., Deschrijver, D., Dhaene, T., 2017. Multi-objective geometry optimization of a gas cyclone using triple-fidelity co-Kriging surrogate models. J. Optim. Theory Appl. 175, 172–193. https://doi.org/10.1007/s10957-017-1114-3.
Soleimani, S., Bozorg-Haddad, O., Boroomandnia, A., Loáiciga, H.A., 2021. A review of conjunctive GW-SW management by simulation–optimization tools. J. Water Supply: Res. Technol.-Aqua 70, 239–256. https://doi.org/10.2166/aqua.2021.106.
Song, J., Yang, Y., Wu, Jianfeng, Wu, Jichun, Sun, X., Lin, J., 2018. Adaptive surrogate model based multiobjective optimization for coastal aquifer management. J. Hydrol. 561, 98–111. https://doi.org/10.1016/j.jhydrol.2018.03.063.
Song, X., Lv, L., Sun, W., Zhang, J., 2019. A radial basis function-based multi-fidelity surrogate model: exploring correlation between high-fidelity and low-fidelity models. Struct. Multidisc. Optim. 60, 965–981. https://doi.org/10.1007/s00158-019-02248-0.
Sreekanth, J., Datta, B., 2010. Multi-objective management of saltwater intrusion in coastal aquifers using genetic programming and modular neural network based surrogate models. J. Hydrol. 393, 245–256. https://doi.org/10.1016/j.jhydrol.2010.08.023.
Sreekanth, J., Datta, B., 2015. Review: simulation-optimization models for the management and monitoring of coastal aquifers. Hydrogeol. J. 23, 1155–1166. https://doi.org/10.1007/s10040-015-1272-z.
Strack, O.D.L., 1976. A single-potential solution for regional interface problems in coastal aquifers. Water Resour. Res. 12, 1165–1174. https://doi.org/10.1029/WR012i006p01165.
Tsoukalas, I., Kossieris, P., Efstratiadis, A., Makropoulos, C., 2016. Surrogate-enhanced evolutionary annealing simplex algorithm for effective and efficient optimization of water resources problems on a budget. Environ. Model. Softw. 77, 122–142. https://doi.org/10.1016/j.envsoft.2015.12.008.
Tyan, M., Nguyen, N.V., Lee, J.-W., 2015. Improving variable-fidelity modelling by exploring global design space and radial basis function networks for aerofoil design. Eng. Optim. 47, 885–908. https://doi.org/10.1080/0305215X.2014.941290.
Ulaganathan, S., Couckuyt, I., Deschrijver, D., Laermans, E., Dhaene, T., 2015. A matlab toolbox for Kriging metamodelling. procedia computer science. In: International Conference On Computational Science, ICCS 2015, 51, pp. 2708–2713. https://doi.org/10.1016/j.procs.2015.05.395.
Viana, F., Haftka, R., Watson, L., 2010. Why Not Run the Efficient Global Optimization Algorithm With Multiple Surrogates?, in: 12th. American Institute of Aeronautics and Astronautics, Orlando, Florida. https://doi.org/10.2514/6.2010-3090.

Wang, C., Duan, Q., Gong, W., Ye, A., Di, Z., Miao, C., 2014. An evaluation of adaptive surrogate modeling based optimization with two benchmark problems. Environ. Model. Softw. 60, 167–179.

Wu, W., Ren, J., Zhou, X., Wang, J., Guo, M., 2020. Identification of source information for sudden water pollution incidents in rivers and lakes based on variable-fidelity surrogate-DREAM optimization. Environ. Model. Softw. 133, 104811 https://doi.org/10.1016/j.envsoft.2020.104811.

Xia, W., Shoemaker, C., 2020. GOPS: efficient RBF surrogate global optimization algorithm with high dimensions and many parallel processors including application to multimodal water quality PDE model calibration. Optim. Eng. https://doi.org/10.1007/s11081-020-09556-1.

Xia, W., Shoemaker, C., Akhtar, T., Nguyen, M.-T., 2021. Efficient parallel surrogate optimization algorithm and framework with application to parameter calibration of computationally expensive three-dimensional hydrodynamic lake PDE models. Environ. Model. Softw. 135, 104910 https://doi.org/10.1016/j.envsoft.2020.104910.

Xiao, C., Tian, L., 2020. Surrogate-based joint estimation of subsurface geological and relative permeability parameters for high-dimensional inverse problem by use of smooth local parameterization. Water Resour. Res. 56, e2019WR025366 https://doi.org/10.1029/2019WR025366.

Yi, J., Shen, Y., Shoemaker, C.A., 2020. A multi-fidelity RBF surrogate-based optimization framework for computationally expensive multi-modal problems with application to capacity planning of manufacturing systems. Struct. Multidisc. Optim. 62, 1787–1807. https://doi.org/10.1007/s00158-020-02575-7.

Yin, J., Tsai, F.T.-C., 2020. Bayesian set pair analysis and machine learning based ensemble surrogates for optimal multi-aquifer system remediation design. J. Hydrol. 580, 124280 https://doi.org/10.1016/j.jhydrol.2019.124280.

Younes, A., Fahs, M., Ahmed, S., 2009. Solving density driven flow problems with efficient spatial discretizations and higher-order time integration methods. Adv. Water Res. 32, 340–352. https://doi.org/10.1016/j.advwatres.2008.11.003.

Yu, X., Sreekanth, J., Cui, T., Pickett, T., Xin, P., 2021. Adaptative DNN emulator-enabled multi-objective optimization to manage aquifer−sea flux interactions in a regional coastal aquifer. Agric. Water Manage. 245, 106571 https://doi.org/10.1016/j.agwat.2020.106571.

Zhang, J., Man, J., Lin, G., Wu, L., Zeng, L., 2018a. Inverse modeling of hydrologic systems with adaptive multifidelity Markov Chain Monte Carlo simulations. Water Resour. Res. 54, 4867–4886. https://doi.org/10.1029/2018WR022658.

Zhang, Y., Han, Z.-H., Zhang, K.-S., 2018b. Variable-fidelity expected improvement method for efficient global optimization of expensive functions. Struct. Multidisc. Optim. 58, 1431–1451. https://doi.org/10.1007/s00158-018-1971-x.

Zheng, Q., Zhang, J., Xu, W., Wu, L., Zeng, L., 2019. Adaptive multifidelity data assimilation for nonlinear subsurface flow problems. Water Resour. Res. 55, 203–217. https://doi.org/10.1029/2018WR023615.

Zhou, Q., Shao, X., Jiang, P., Gao, Z., Wang, C., Shu, L., 2016. An active learning metamodeling approach by sequentially exploiting difference information from variable-fidelity models. Adv. Eng. Inf. 30, 283–297. https://doi.org/10.1016/j.aei.2016.04.004.

Zhou, Q., Wu, Y., Guo, Z., Hu, J., Jin, P., 2020. A generalized hierarchical co-Kriging model for multi-fidelity data fusion. Struct Multidisc Optim 62, 1885–1904. https://doi.org/10.1007/s00158-020-02583-7.

Asher, M.J., Croke, B.F.W., Jakeman, A.J., Peeters, L.J.M., 2015. A review of surrogate models and their application to groundwater modeling. Water Resour. Res. 51, 5957–5973. https://doi.org/10.1002/2015WR016967.